IEEE Access
Multidisciplinary | Rapid Review | Open Access Journal

Received January 30, 2021, accepted February 17, 2021, date of publication February 22, 2021, date of current version March 4, 2021.

Digital Object Identifier 10.1109/ACCESS.2021.3060935

General Classification and Comprehensive Performance Assessment of Multi-Objective DC Voltage Control in Multi-Terminal HVDC Networks

SAWSAN S. SAYED AND AHMED M. MASSOUD, (Senior Member, IEEE)
Department of Electrical Engineering, Qatar University, Doha, Qatar
Corresponding author: Sawsan Sayed (ssayed@qu.edu.qa)

This work was supported by the National Priorities Research Program (NPRP) through the Qatar National Research Fund under Grant 9-092-2-045. Open Access funding was provided by the Qatar National Library.

ABSTRACT The recent massive global movement towards green energy in power systems has raised the efforts of integrating large-scale Renewable Energy Sources (RESs) through Multi-Terminal HVDC (MTDC) systems. The configuration of the MTDC system and the possibility of transnational interconnection impose some challenges and raise the potential of single or multi-objective control for the DC voltage control. Additional requirements from the Transmission System Operator (TSO) and/or AC grids may influence the action taken for the DC voltage control. In this paper, a generalized classification for the DC voltage control methods in an MTDC system is delivered. The DC voltage control methods are classified into conventional control (i.e., reference voltage-based control) and non-conventional control (i.e., virtual resistance-based control) methods. The DC voltage control objective may cover a range of the following targets: power-sharing based on converters' rating capacity, ratio priority of the power distribution, available headroom, and/or loading factor. The control objective may include transmission losses minimization of the MTDC system with optimal or sub-optimal power flow. The design approaches of the control methods for post-contingency operation are presented. The control methods are evaluated and simulated with a 4-terminal radial MTDC network during normal and abnormal system operation. A comprehensive performance assessment is also presented considering the control methods from the perspective of the control method and objective, system efficiency, grid-code violation, communication requirement, and design complexity and flexibility.

INDEX TERMS DC power flow, DC voltage control, HVDC, MTDC, renewable energy source, steady-state.

NOMENCLATURE

AHD	Available headroom-based droop.
FDCT	Flexible DC transmission.
FRD	Fixed rating-based droop.
GSC	Grid-side converter.
LFD	Loading factor-based droop.
M/S	Master/slave.
MTLD	Minimum transmission loss-based droop.
OPF	Optimal power flow.
RPD	Ratio priority-based droop.
SCADA	Supervisory control and data acquisition.
TSO	Transmission system operator.
TSOD	TSO-based droop.
VM	Voltage margin.
WSC	Wind-side converter.
K	Droop gain.
P	DC power.
R	DC transmission line resistance.
V	DC voltage.
Subscripts	
wi	i_{th} WSC.
gj	j_{th} GSC.

The associate editor coordinating the review of this manuscript and approving it for publication was Ramazan Bayindir.

I. INTRODUCTION

Renewable Energy Sources (RESs) are the modern advances in mainstream high-power transmission systems. The uninterruptible power supply and clean generation nature of the RESs embolden their steadfastness alongside the worldwide electricity demand and the United Nations' (UN) 2030 sustainable development goals [1], [2]. Due to the nature of the high-power RESs, its installation location is commonly in isolated off-load lands. In recent years, and with the development of fast control power electronics and low-loss high-voltage DC cables, High-Voltage Direct Current (HVDC) and Multi-Terminal HVDC (MTDC) networks with Voltage Source Converters (VSCs) have been the superlative technology for long-distance RESs and transnational power transmission systems [3]. Regardless, RESs interconnection with HVDC-links degrades the system inertia. Furthermore, the intermittent power supply nature from the RESs requires extensive and regular AC/DC power/voltage management [4], [5].

A substantial measurement-index for supply/load balance and management of an MTDC network is the DC voltage stability. Wide-range studies have been conducted on the load flow and steady-state/dynamic operation of MTDC systems [6]–[9]. Also, various DC voltage control schemes have been proposed, via a hierarchical control structure, for the power/voltage management of the MTDC network. Further detailed elaboration about the development of the hierarchical layers of MTDC networks is available in [5], [10]–[18]. Moreover, power flow control in transmission lines of MTDC networks has been addressed in [19] and [20] by introducing Flexible DC Transmission (FDCT) with high-power DC-DC converters. The FDCT concept has been expanded in [21] for multi-purpose power/voltage management of MTDC systems (e.g., voltage level matching, line flow control, and voltage boosting). Although several DC voltage control methods have been suggested in literature addressing the DC-side stability of an MTDC system; however, a comprehensive up-to-date review of these control methods has not been presented.

This paper aims to present a comprehensive performance assessment of various DC voltage control methods in MTDC networks. A generalized classification of the DC voltage control techniques in an MTDC system is presented in Fig. 1. The DC voltage control methods are classified into conventional control (i.e., reference voltage-based control) and non-conventional control (i.e., virtual resistance-based control) methods. This paper presents and assesses several control schemes based on their design approach and steady-state load flow performance while focusing on the DC-side operation. The performance evaluation is verified with a 4-terminal MTDC network. Each approach's merits and demerits are evaluated and presented from the perspective of normal system operation and stable post-contingency operation. A graphical illustration of the paper is presented in Fig. 2. The contribution of the paper can be shortlisted as follows.

TABLE 1. Summary of decentralized control layers in MTDC networks.

Control Layer	Decentralized Layers	
	Outer Controller	**Inner Controller**
Functions/ Objectives	General DC Control Modes: Power, Voltage, and/or Current Control.	Synchronize the VSC Voltage with the AC Grid.
	-Respond to Power Imbalance Locally. -Saturate Power and Current for VSC Limitations. -Independent Active and Reactive Power Control.	
Construction	Vector Control, PI Controller, and PLL.	
Inputs	-V^*_{DC} and P^*_{DC}. -Control Characteristics.	-i^*_d, i^*_q, i_d, i_q, v_d, v_q, ω and L_T.
Outputs	i^*_d and i^*_q.	$v^*_{t,d}$ and $v^*_{t,q}$.
Communication	Possible Required (Based on Outer Control Scheme).	
Time Constant	Tens of Milliseconds.	

Where PI refers to Proportional-Integral, PLL refers to Phase-Locked Loop. V^*_{DC} and P^*_{DC} are the reference DC voltage and power, respectively, of the VSC. i^*_d, i^*_q, $v^*_{t,d}$, and $v^*_{t,q}$ are the reference AC current and voltage of the VSC in the dq frame. v_d and v_q are the AC grid voltage in the dq frame. ω and L_T are the AC grid angular frequency and line filter, respectively.

- Provide a comprehensive background of different DC voltage control methods, conventional and non-conventional-based, for an MTDC network.
- Investigate the design approach and steady-state performance of DC voltage controllers in an MTDC network.
- Conduct a performance assessment among the entailed DC voltage control methods for an MTDC network, considering case studies.

The structure of the paper is as follows. Section II gives an overall view of the MTDC network's control structure. Section III presents conventional-based DC voltage control techniques in MTDC networks. Section IV presents non-conventional-based DC voltage control methods in MTDC systems. Section V delivers case studies for the presented control methods. Section VI presents an evaluation and performance assessment of the covered DC voltage controllers. Finally, section VII gives an overall summary of the presented work.

II. MTDC NETWORKS: UNIVERSAL CONTROL STRUCTURE

A. HIERARCHICAL CONTROL LAYERS

The general structure of an MTDC system and its hierarchical control layers are presented in Fig. 3, considering the Wind-Side Converters (WSCs) as rectifiers, while the Grid-Side Converters (GSCs) as inverters. The lack of inertia in MTDC systems results in fast DC voltage fluctuations. Therefore, during disturbances (e.g., RESs supply variations, line/converter outages, and/or faults), fast action controllers are required [10]. The universal proposed control layers of MTDC systems consist of high-level or centralized control layers (i.e., supervisory and tertiary layers) and low-level or decentralized control layers (i.e., outer and inner controllers) [5], [10]–[18]. A summary of the control layers is presented in TABLE 1 and TABLE 2 [5], [10], [13], [18], [22]–[24].

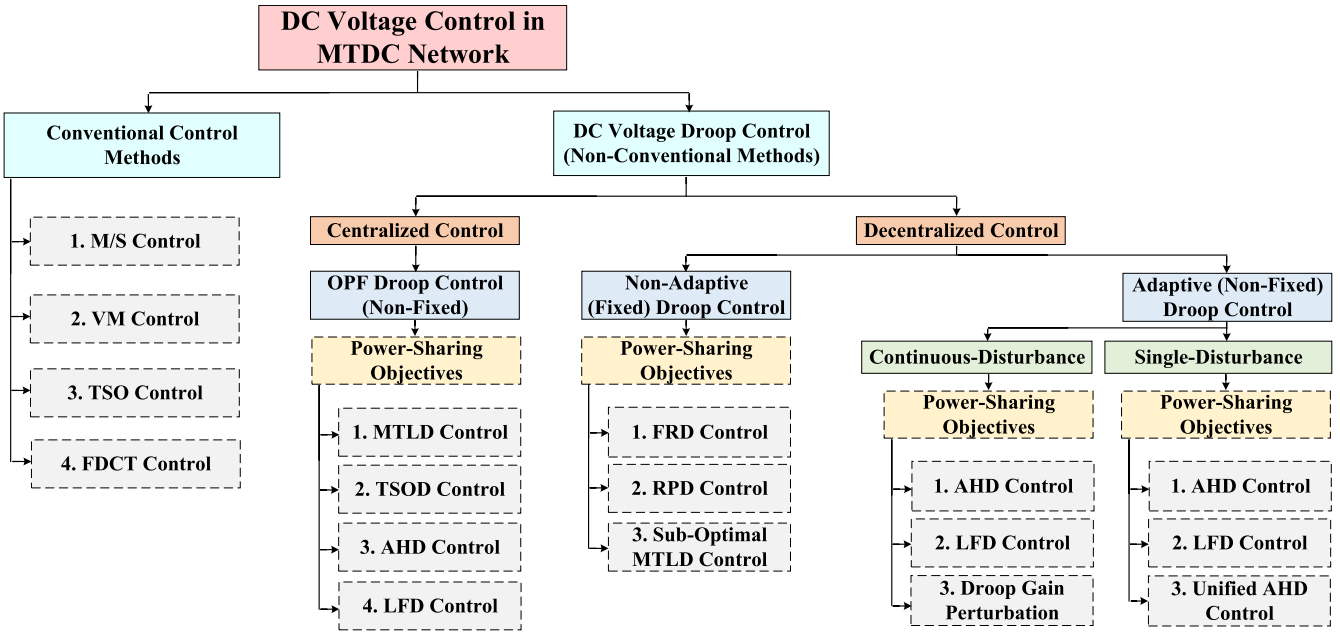

FIGURE 1. Classification of the DC voltage control in an MTDC system, where the abbreviations stand for the following: Master/Slave (M/S), Voltage Margin (VM), Transmission System Operator (TSO), Flexible DC Transmission (FDCT), Optimal Power Flow (OPF), Minimum Transmission Loss-based Droop (MTLD), TSO-based Droop (TSOD), Available Headroom-based Droop (AHD), Loading Factor-based Droop (LFD), Fixed Rating-based Droop (FRD), and Ratio Priority-based Droop (RPD).

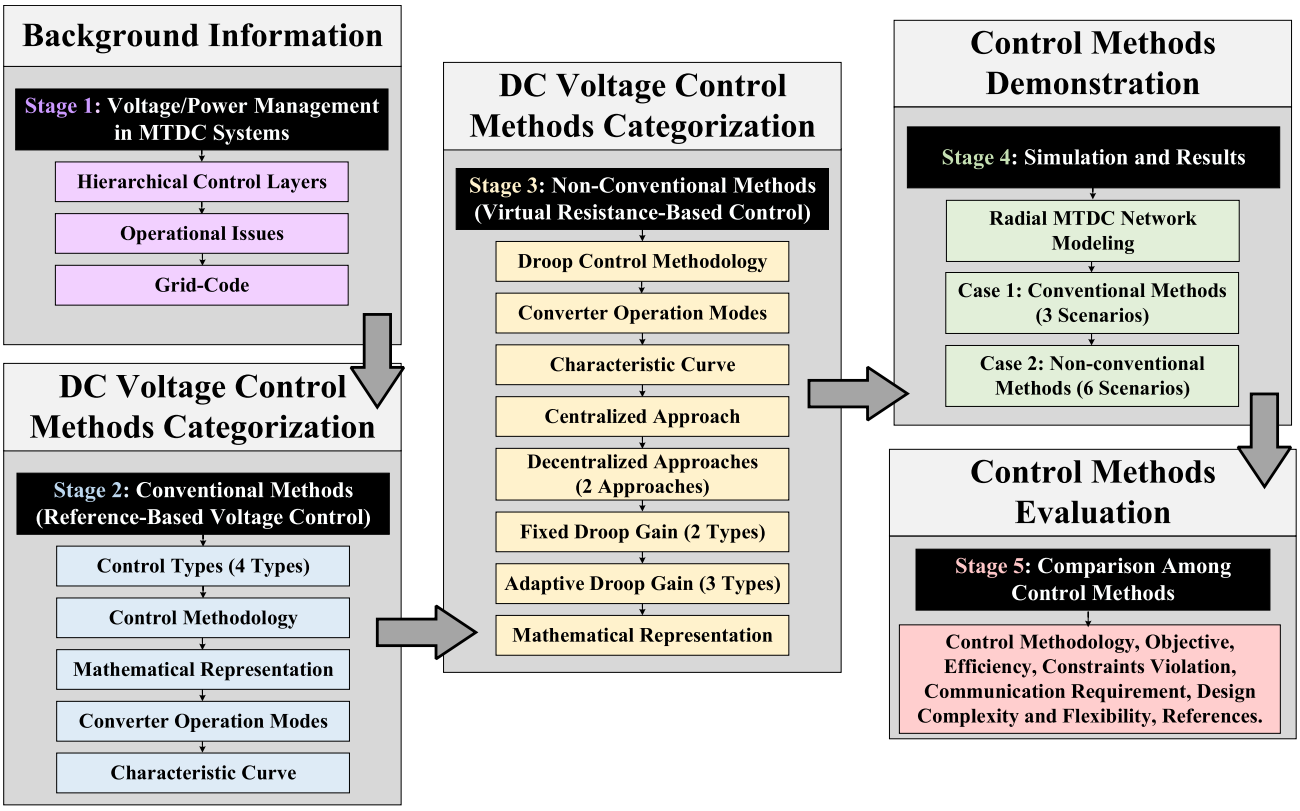

FIGURE 2. Graphical diagram of the paper flow.

B. OPERATIONAL ISSUES AND CONSTRAINTS

The load flow balance is essential for stable MTDC system operation. However, with the intermittent characteristics of the RESs, it is difficult to evade unbalanced events as 100% forecasting accuracy cannot be guaranteed [25]. In such a case, energy storage can be considered for deployment to

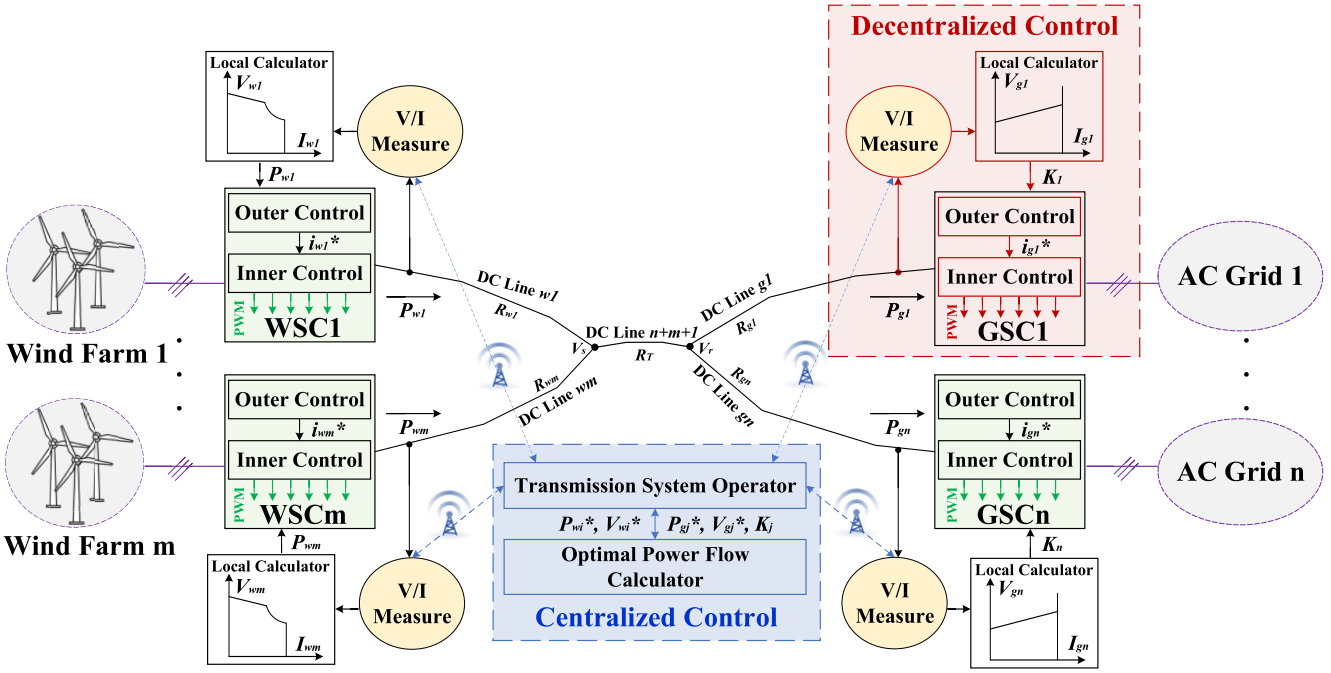

FIGURE 3. MTDC network configuration with a hierarchical control structure, where P_{wi}, V_{wi}, and I_{wi} are the DC power, voltage, and current, respectively, of the i^{th} WSC, while P_{gj}, V_{gj}, I_{gj}, and K_j are the DC power, voltage, current, and droop gain, respectively, of the j^{th} GSC. R_{wi} and R_{gj} are the resistance of the DC transmission line connected to the i^{th} WSC and j^{th} GSC, respectively. R_T is the resistance of the DC transmission line that carries the total power received from the WSCs.

TABLE 2. Summary of centralized control layers in MTDC networks.

Control Layer	Centralized Layers	
	Secondary Controller	Tertiary Controller
Functions/ Objectives	-Update P^*_{DC} based on the Tertiary Layer. -Restore Power Balance after a Disturbance. -Validate Measurements. -OPF.	Schedule P^*_{DC} based on Economical, Technical, and/or TSOs Requirements.
Construction	Centralized SCADA.	Global SCADA.
Inputs	-Conductance Matrix of the MTDC System. -Measurements from the Decentralized Layer.	
	-Operating Constraints from TSO of MTDC System. -P^*_{DC}.	Operating Constraints from TSOs of AC Grids.
Outputs	V^*_{DC}, P^*_{DC}, and/or Control Characteristics.	V^*_{DC} and/or P^*_{DC}.
Communication	Required.	Required.
Time Constant	Tens of Seconds.	20 Minutes to 1 Hour.

Where SCADA refers to Supervisory Control and Data Acquisition.

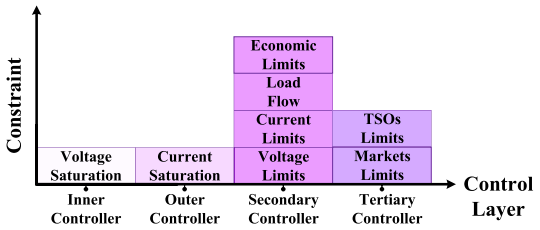

FIGURE 4. General constraints of the hierarchical control layers in an MTDC network.

evade the deviation between the generation and demand [25]. Nevertheless, this is an expensive solution for mitigating the forecasting error. Another approach for achieving the balance between the generation and load in a short time is the optimization of the deviated power delivery to an alternative load with the lowest market price [25].

The general required constraints of the hierarchical control layers for an MTDC network are shown in Fig. 4. Well-coordinated DC voltage control attains balanced power flow among the GCSs in an MTDC network. Excessively high-level voltages above the nominal network voltage may cause activation of the protective equipment (e.g., DC damping resistors). Meanwhile, voltage deterioration to low-levels may limit controllers' capabilities [26], [27]. To overcome the DC over-voltage, some approaches have been proposed as the local DC chopper installation in the MTDC grid and/or power reduction of wind turbines in the case of wind farm-connected RESs through local control and/or fast communication [28]. A generic protocol for DC voltage control design includes two main aspects: reliability during system disturbances (i.e., autonomous control action) and system/equipment constraints (e.g., converter and line ratings) [24], [29]. In addition, the allowed standard operating-range of DC grid voltages is set between ±5% to ±10% of the nominal network voltage [13]. Furthermore, an additional preferable protocol is to operate the MTDC system at the highest

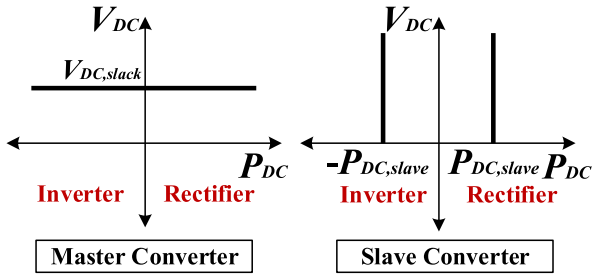

FIGURE 5. Characteristic curves for the M/S control, where $V_{DC,slack}$ is the reference DC voltage for the master converter, and $P_{DC,slave}$ is the reference power for the slave converter.

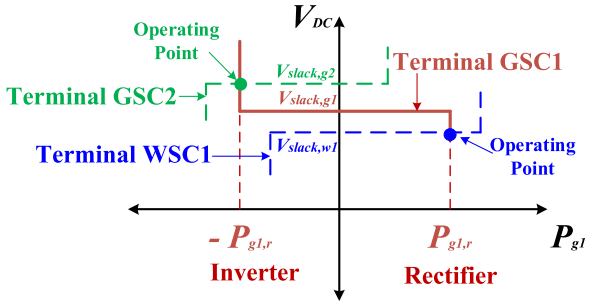

FIGURE 6. Characteristic curves for the VM control, where $V_{slack,g1}$, $V_{slack,g2}$, and $V_{slack,w1}$ are the reference DC voltages of GSC1, GSC2, and WSC1, respectively, during the master control mode.

allowed DC voltage (i.e., reduced transmission losses) for OPF and economic benefits [14], [30], [31].

In this paper, the common proposed DC voltage control techniques in the literature are classified into conventional-based control (i.e., reference voltage-based control) and non-conventional-based control (i.e., virtual resistance-based control) methods, as shown in Fig. 1. Further details are presented in the subsequent sections.

III. DC VOLTAGE CONTROL CATEGORIZATION: CONVENTIONAL METHODS

A. MASTER/SLAVE (M/S) CONTROL

The M/S control scheme, also named as the centralized DC slack-bus control, allows one VSC, the master converter, to take the role of DC voltage control in constant control mode, while the rest of the VSCs, slave converters, operate in the constant power control mode, as elaborated in Fig. 5. The master converter supplies or absorbs any power imbalance of the entire DC network. Therefore, the power balance of the system depends on the availability and capabilities of the master converter [24], [26], [29]. In [6], a power flow solution of an MTDC network with M/S control is presented. For an MTDC network with m WSCs and n GSCs, with GSC1 acting as the master converter, while the rest of the VSCs acting as slave converters, then (1) must be guaranteed for balanced power flow during any disturbance event.

$$P_{g1,r} \geq \sum_{j=2}^{n} P_{gj} + \sum_{i=1}^{m} P_{wi} \tag{1}$$

where $P_{gj,r}$ is the power rating of the j^{th} GSC (e.g., $P_{g1,r}$ is the power rating of GSC1).

This control scheme works well with a large MTDC network under small power injection fluctuations, as demonstrated in [32]. However, in large disturbance events, the master converter may not restore the system balance due to its power rating limitation. The master converter's failure due to an outage reduces this control scheme's reliability during critical situations [29]. Moreover, fast communication is required between the master converter and slave converters after a system blackout [33]. To avoid DC grid power flow imbalance or outage due to the master converter power rating limitation or disconnection, a back-up converter is required to take over the role of the DC voltage control. To achieve that, the next control scheme was introduced.

B. VOLTAGE MARGIN (VM) CONTROL

The VM control technique is an enhanced version of the M/S control scheme, such that, aside from the master converter, the DC voltage control can be attained with an alternative converter. This control scheme is activated when the master converter violates its references DC voltage [24], [29], [34]. In this method, similarly to the M/S control, one converter is responsible for the DC voltage control, while the rest of the converters act in constant power control mode. However, if the master converter cannot balance the power flow, another converter takes the slack-bus role.

For example, consider a 3-terminal MTDC network with VSC terminals GSC1, GSC2, and WSC1, where initially terminal GSC1 is the master converter, as presented in Fig. 6 GSC1 acts as the slack-bus as long as it does not reach its maximum power injection limit. If GSC1 exceeds its power injection limit in the inverter mode, then the reference DC voltage increases above $V_{slack,g1}$, until reaching the other converter's reference DC voltage, $V_{slack,g2}$, which will become the slack-bus. While if GSC1 reaches its maximum power injection in the rectifier mode, then the reference DC voltage, $V_{slack,g1}$, is decreased until reaching the reference voltage of WSC1, $V_{slack,w1}$, and WSC1 will start to act as the master converter. In (2), the 3-terminal MTDC network operation is expressed in terms of the net power flow.

$$\begin{aligned} &\text{If } V_{g1} = V_{slack,g1} \therefore\ P_{g1,r} \geq P_{g2} + P_{w1} \\ &\text{If } V_{g1} < V_{slack,g1} \therefore\ P_{w1,r} \geq P_{g1} + P_{g2} \\ &\text{If } V_{g1} > V_{slack,g1} \therefore\ P_{g2,r} \geq P_{g1} + P_{w1} \end{aligned} \tag{2}$$

where $P_{wi,r}$ is the power rating of the i^{th} WSC (e.g., $P_{w1,r}$ is the power rating of WSC1).

This control method's main issue is controlling the DC network voltage with a single converter through the slack-bus swapping. In addition, the number of possible slack-buses may be limited by the DC voltage operating range that is $\pm 10\%$ of the nominal network voltage [33].

C. TRANSMISSION SYSTEM OPERATOR (TSO) CONTROL

The management of an MTDC network requires interaction among different TSO entities for data exchange and power flow coordination. Several possible TSO architectures may exist for the operational responsibility of the MTDC grid, such as independent, distributed, and integrated architectures [5]. However, regardless of the TSO control architectures, the power flow control in the MTDC grid can achieve a power distribution based on the market economic interest, secure contingency events, and/or optimized load flow [25], [35].

A smart approach of DC voltage control can offer supplementary actions on the power flow, aside from secure operation, that can optimize the load flow based on certain criteria and constraints. The Distributed Voltage Control (DVC) technique allows multiple GSCs to share the responsibility of DC voltage control based on the supplied reference DC voltage from the secondary control layer [33], [36], [37]. DC power flow needs to be performed regularly to obtain the required set-points. OPF is the common approach for the DVC method.

The optimization process by the OPF of the MTDC system includes presenting a mathematical representation of the system, identify the variables and constraints that the network must meet at all times, and define the system properties for which the state of the optimization will be maximized or minimized [38], [39]. Several optimization techniques have been proposed in the literature that can be classified as classical and metaheuristics methods. Further elaboration about the optimization methods is available in [38], [39], and [40].

The objective function that has been commonly employed for MTDC grids is based on a combination of transmission line losses, VSCs losses, and DC-DC converters losses minimization [19]–[21]. A high-power DC-DC converter can be employed in MTDC systems for several purposes, as will be elaborated in the next section. A general mathematical representation for an optimization function and constraints can be written as follows, in terms of the network DC voltages.

$$\begin{aligned} &\min F(\boldsymbol{V_{DC}}) \text{ such that} \\ &\boldsymbol{N}(\boldsymbol{V_{DC}}) \leq 0 \text{ and} \\ &\boldsymbol{E}(\boldsymbol{V_{DC}}) = 0 \end{aligned} \tag{3}$$

where F is the optimization return solution. $\boldsymbol{V_{DC}}$ is a vector of the DC grid nodes voltage. $\boldsymbol{N}$ and $\boldsymbol{E}$ are the inequality and equality constraint vector functions, respectively.

A summary of the optimization function and constraints for an overall MTDC system is presented in (4)-(7).

$$P_{obj} = P_{TL} + P_{VSC} + P_{DC-DC} \tag{4}$$

where P_{obj} is the optimization function for the OPF of an MTDC network. P_{TL} is the transmission lines' power losses. P_{VSC} is the VSCs power losses. P_{DC-DC} is the DC-DC converters power losses.

$$P_{TL} = \sum_{i=1}^{l} I_{L,i}^2 R_{L,i} \tag{5}$$

where l is the number of DC transmission lines in the MTDC grid. R_L is the DC line resistance. I_L is the DC line current flow.

$$\begin{aligned} P_{VSC} &= \sum_{i=1}^{p} P_{nl,i} + V_{VSC,i} I_{AC,i} + R_{VSC,i} I_{AC,i}^2 \\ \text{and } I_{AC,i} &= \frac{P_{in,i}}{\sqrt{3} V_{AC,i}} \end{aligned} \tag{6}$$

where P_{nl} is the no-load power losses. V_{VSC} is the linearly-dependent losses in Volt. R_{VSC} is the quadratically-dependent losses term in Ohm. The AC-side voltage and current flow are represented by V_{AC} and I_{AC}, respectively. P_{in} is the input power to the VSC. $p = n + m$ (i.e., p is equivalent to the total number of VSCs in the MTDC network).

$$\boldsymbol{X_{min}} \leq \boldsymbol{X} \leq \boldsymbol{X_{max}} \tag{7}$$

where $\boldsymbol{X} = [\boldsymbol{V_{DC}}, \boldsymbol{P_{DC}}, \boldsymbol{I_{DC}}, \boldsymbol{I_L}]^T$. $\boldsymbol{P_{DC}}$ is a vector of the VSCs injected/or received power. $\boldsymbol{I_{DC}}$ is a vector of the VSCs injected/ or received current. $\boldsymbol{I_L}$ is a vector of the transmission lines' current flow. $\boldsymbol{X_{max}}$ and $\boldsymbol{X_{min}}$ represent the maximum and minimum ranges of the variable $\boldsymbol{X}$, respectively.

The high-power DC-DC converters losses, P_{DC-DC}, can be considered in a similar manner to the VSC, with a front-to-front DC-DC converter (i.e., two VSCs) [21], [41].

For a radial MTDC network, based on Fig. 3, the constraints and P_{TL} can be rewritten as follows.

$$\begin{aligned} P_{TL} = \left(\sum_{i=1}^{m} (V_{wi} - V_s)^2 G_{wi}\right) + (V_s - V_r)^2 G_T \\ + \left(\sum_{j=1}^{n} (V_r - V_{gj})^2 G_{gj}\right) \end{aligned} \tag{8}$$

where $G_{wi} = 1/R_{wi}$, $G_{gj} = 1/R_{gj}$, and $G_T = 1/R_T$.

$$\boldsymbol{V_{min}} \leq \boldsymbol{V_{DC}} \leq \boldsymbol{V_{max}} \tag{9}$$

where $\boldsymbol{V_{DC}} = [V_{w1}, \ldots, V_{wm}, V_s, V_r, V_{g1}, \ldots, V_{gn}]^T$. $\boldsymbol{V_{max}} = [1.05pu, \ldots, 1.05pu]^T$. $\boldsymbol{V_{min}} = [0.95pu, \ldots, 0.95pu]^T$. $\boldsymbol{V_{max}}$ and $\boldsymbol{V_{min}}$ are of the size $m + n + 2$, assuming operating the MTDC grid around $\pm 5\%$ of the nominal network DC voltage.

$$-\boldsymbol{P_{max}} \leq \boldsymbol{P_{DC}} \leq \boldsymbol{P_{max}} \tag{10}$$

where $\boldsymbol{P_{DC}} = [P_{w1}, \ldots, P_{wm}, P_{g1}, \ldots, P_{gn}]^T$. $\boldsymbol{P_{max}} = [P_{w1,r}, \ldots, P_{wm,r}, P_{g1,r}, \ldots, P_{gn,r}]^T$.

$$-\boldsymbol{I_{max}} \leq \boldsymbol{I_{DC}} \leq \boldsymbol{I_{max}} \tag{11}$$

where $\boldsymbol{I_{DC}} = [I_{w1}, \ldots, I_{wm}, I_{g1}, \ldots, I_{gn}]^T$.
$\boldsymbol{I_{max}} = [I_{w1,r}, \ldots, I_{wm,r}, I_{g1,r}, \ldots, I_{gn,r}]^T$. $I_{wi,r}$ and $I_{gj,r}$ are the current rating of the i^{th} WSC and j^{th} GSC, respectively.

$$-\boldsymbol{I_{L,max}} \leq \boldsymbol{I_L} \leq \boldsymbol{I_{L,max}} \tag{12}$$

where $\boldsymbol{I_L} = [I_{w1}, \ldots, I_{wm}, I_T, I_{g1}, \ldots, I_{gn}]^T$. $\boldsymbol{I_{L,max}}$ is a vector for the maximum current rating of the DC transmission lines with size $n + m + 1$.

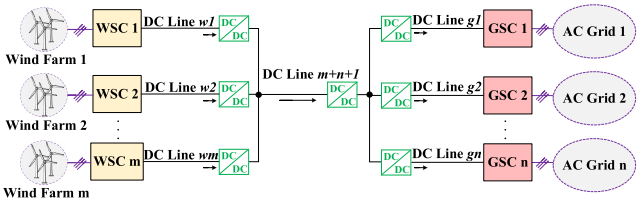

FIGURE 7. High-power DC-DC converter integration with a radial MTDC network for FDCT and/or DC voltage level matching.

The load flow constraint of the radial MTDC network is as follows.

$$\left(\sum_{i=1}^{m}\frac{V_{wi}-V_s}{R_{wi}}\right)+\left(\sum_{j=1}^{n}\frac{V_r-V_{gj}}{R_{gj}}\right)=2\frac{V_s-V_r}{R_T} \quad (13)$$

D. FLEXIBLE DC TRANSMISSION (FDCT) CONTROL

The input or output power control of MTDC networks is commonly achieved via the VSCs. While the power flow in the transmission lines may not be controlled without external equipment (e.g., DC-DC converter [19], [20], [21] and/or interline DC power flow controller [42]). Therefore, FDCT control has been introduced to MTDC systems via high-power DC-DC converters to allow voltage level matching among the different operating DC voltage systems, interconnection between the different MTDC configurations, and/or control the power flow in the DC transmission lines [21]. In [19] and [20], integrating a high-power DC-DC converter into an MTDC system has been explored for transmission loss minimization and power flow regulation, respectively. In addition, in [21], the OPF in MTDC networks has been investigated with a high-power DC-DC converter integration while considering the DC voltage nodes enhancement, DC voltage level matching, and flexible power transmission with radial and mesh systems. The high-power DC-DC converter can regulate the DC voltage drops in the MTDC network, regardless of the RESs generation variations, to allow efficient power transmission. That is, by regulating the DC voltage at a critical node to the highest allowed operating voltage, 1.05 pu, with respect to its base voltage [21]. A possible integration scheme of the high-power DC-DC converter into a radial MTDC network is presented in Fig. 7, while further details are available in [21]. For DC nodes voltage enhancement, the high-power DC-DC converter gain, D, can be controlled as follows [21].

$$D=\frac{V_{out}}{V_{in}} \text{ for } V_{out}=1.05 \text{ pu } \forall t \quad (14)$$

where V_{out} and V_{in} are the output and input DC voltages of the high-power DC-DC converter, respectively. t refers to time.

IV. DC VOLTAGE CONTROL CATEGORIZATION: NON-CONVENTIONAL METHODS

A. INTRODUCTION: VIRTUAL RESISTANCE CONTROL

For autonomous control action and condensed communication reliability, the DC voltage droop control has been introduced [6], [12], [13], [29], [41], [43]. To regulate the DC voltage during a normal MTDC network operation, several GSCs can be set to droop control mode for power imbalance management with simultaneous GSCs' control actions [27]. The DC power and voltage of the GSC varies based on the designed droop characteristic (i.e., a virtual resistance behavior) [10]. The power-sharing variations and DC voltage differences among the GSCs, in an MTDC network, can appear due to the DC lines resistances, droop gains, and/or measurement errors [44]–[46]. The power flow formulation of a droop-controlled MTDC network has been covered in [6].

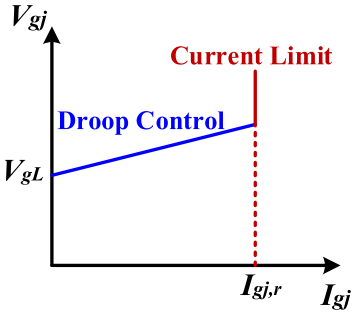

FIGURE 8. A general droop characteristic curve for a GSC.

The droop characteristic curve for a GSC in an MTDC network is shown in Fig. 8. In case the converter reaches its maximum converter rating due to system disturbance, the control mode can move to the current limit mode.

For the radial MTDC network in Fig. 3, the GSCs-side load flow equations can be rewritten in droop control mode as follows, during steady-state operation, $\forall j \in [1,\ldots,n]$.

$$\begin{aligned} V_{gj} &= I_{gj}K_j + V_{gL} \text{ and} \\ V_{gj} &= V_r - I_{gj}R_{gj} \end{aligned} \quad (15)$$

where V_{gL} is the no-load DC voltage of the DC grid.

$$\left(\sum_{i=1}^{m}\frac{V_{wi}-V_s}{R_{wi}}\right)+\left(\sum_{j=1}^{n}\frac{V_r-V_{gL}}{R_{gj}+K_j}\right)=2\frac{V_s-V_r}{R_T} \quad (16)$$

While for droop-controlled GSC, the following is achieved.

$$V_{gj}=V_{gL}+(1/K_j)(P^*_{gj}-P_{gj}) \quad (17)$$

where P^*_{gj} is the reference DC power for the j^{th} GSC.

The DC voltage droop control is similar to the DVC method in terms of distributing the DC voltage control responsibility among several converters. Therefore, it is not required for the converters to be oversized in terms of power rating. It is also unnecessary to provide a back-up converter, in contrast to the M/S and VM control techniques [18]. The droop control can operate locally without communication via the secondary control layer, with stable MTDC operation. However, for OPF operation, the droop gains require regular updates based on the accurate power input fluctuations from the RESs [14]. Moreover, with decentralized droop control, in case of line and/or converter outage, the post-contingency

power flow does not follow the reference set points [18], [24]. Another drawback of the droop control is that it does not allow to operate in constant DC voltage or power control modes during power flow fluctuation. However, this point has been advised by a Generalized Voltage Droop (GVD) control technique, which allows to alternate between the DC voltage droop control, constant DC voltage control, and constant DC power control modes [45].

Also, modified DC voltage droop control schemes have been proposed, such as the dead-band and undead-band droop control techniques [24], [29], [47].

The DC voltage droop control structure of an MTDC system can be achieved with two approaches, centralized-based, and decentralized-based control, as presented in the next sections.

B. CENTRALIZED-BASED DC VOLTAGE DROOP CONTROL

The centralized-based DC voltage droop control method can be considered an extension of the TSO control with an external virtual resistance at the outer control layer as a proportional controller for local DC voltage control action. The droop gain of the j^{th} GSC can be calculated based on the desired power flow objective (e.g., OPF for MTDC system losses minimization as presented in section III-C), as follows.

$$K_j = \frac{V_{gj} - V_{gL}}{I_{gj}} \tag{18}$$

where V_{gj} and I_{gj} can be obtained by the OPF.

The update frequency of the droop gains can be controlled by the OPF calculation. The droop gains can remain fixed at the outer control layer unless the DC voltage exceeds the specified limit. In that case, the optimization algorithm needs to optimize the droop reference value under power injection variations [6], [14]. In [11], a centralized-based DC voltage droop control has been proposed. The droop gains are updated regularly within a time interval of one hour with the MTDC system's objective and AC grid losses minimization. Hence, the power and voltages of the MTDC network are regulated without extensive communication among the control layers. Similar studies of centralized-based DC voltage droop control for MTDC systems have been presented in [12], [13], [14], [17], and [48]. Moreover, several studies covered the design of the droop gains for OPF and/or sub-optimal power flow [30], [37], [49].

Another critical factor that can alter the droop gains' updates by the OPF calculator is the unforced and/or forced system parameter variations. This refers to the impact of the RESs' power variations and DC line resistances uncertainty on the droop gain tuning, as unforced parameter variations. In addition, the impact of the communication threats (i.e., cyber-attacks) on the adjustment of the droop gains, as forced parameter variations. These issues have been tackled from various points of view, including MTDC system stability and economics, in [31], [41], [44], and [50]. However, in [41], the impact of the unforced parameter variations in an MTDC network is observed considering the DVC approach rather than the centralized-based DC voltage droop control.

C. DECENTRALIZED-BASED DC VOLTAGE DROOP CONTROL

Local and fast autonomous control action on the DC voltages of the MTDC system is essential to avoid triggering the external protection equipment (e.g., damping resistors) and elude system shut-down due to overrating operation. The droop gain adjustment determines the power-sharing among the GSCs. Identical droop gains result in an equivalent power-sharing among the converters [51]. The computation of the droop coefficient can be obtained for a fixed or adaptive tuning [51]. Unlike the centralized-based DC voltage droop control, this control approach relies on local signals with distributed data acquisition data structure [15]. The droop gain's tuning objective depends on the MTDC system requirements and operating conditions, as elaborated in the next sections. The droop gain design's important aspects include ensuring acceptable converter power margin usage, acceptable DC voltage deviation, and stable MTDC system operation [52].

1) FIXED DROOP CONTROL (NON-VARIABLE GAIN)

Several types of fixed droop control have been proposed based on single-update, or fixed, droop gains for MTDC networks. Some studies have tackled the droop gain design for issues such as AC and/or DC system dynamic stability [53], [54], [55], frequency support [56], [57], and DC voltage deviation [55], [58], [59]. The main objectives of the fixed droop gain tuning, for steady-state MTDC system stable operation, have been the converters' rating limitation (Type 1), power flow, and power-sharing control among converters (Type 2), and DC transmission lines losses minimization (Types 3). These three types are elaborated below.

Type 1: Fixed Rating-Based Droop (FRD) Control

In the case of unequal GSCs rating, the power-sharing among the converters can be adjusted to allow the highest rated converter to share more power compared to the rest of the converters [51], [56]. This is achieved by the FRD control, which imposes an inverse proportional relationship between the droop gain and power rating of the respective converter, as shown in (19) and (20) [56]. If it is desired to limit the converter rating usage to a specific ratio, the term Reserved Power (*RP*) in (20) can be increased to reduce the converter's power-sharing contribution.

$$K_j^{(t)} = K_j^{(t_0)} \frac{\sum_{a=1}^{n} H_a}{H_j} \quad a \neq j \tag{19}$$

$$H_j = P_{gj,r} - RP_j \tag{20}$$

where RP_j is the reserved power (MW) of the j^{th} GSC. H_j is the available power rating of the j^{th} GSC. $K_j^{(t_0)}$ is the initial droop gain of the j^{th} GSC, such that $K_1^{(t_0)} = K_j^{(t_0)} \forall j$.

An alternative possible mathematical calculation for the FRD control, with less computational parameters, is

presented in (21).

$$K_j^{(t)} = K_j^{(t_0)} \frac{MR}{H_j} \tag{21}$$

where $MR = \max(P_{gj,r})$ is the maximum power rating among the GSCs.

Regardless of the RESs variations or MTDC system disturbances, the droop gain $K_j^{(t)}$ in (19) or (21) remains fixed at all times for all the GSCs. Therefore, the FRD control scheme can raise issues regarding the converter overloading and DC voltage rating violation [60]. If the GSC reaches the maximum power rating or DC voltage limit, then the control mode shifts from the DC voltage droop control mode to the constant power control mode or the constant DC voltage mode.

Type 2: Ratio Priority-Based Droop (RPD) Control

The power flow of the MTDC system has continuous fluctuations due to the nature of the RESs. The power variations received by the onshore AC grids (i.e., GSCs) can be imposed on restrictions by the TSO, such that some AC grids can have power-sharing priority over the other AC areas [24], [61]. The RPD control establishes a power ratio for the droop-controlled converters to share the generated power based on the set ratio. Therefore, a ratio tuning factor, r, can be introduced to the GSCs droop gains to control the power-sharing based on the desired power flow. For a case of two GSCs in a radial MTDC network configuration, as in Fig. 3, the droop gains computation with RPD control is obtained for a power-sharing ratio, r, as shown in (22)-(25). The load flow at the GSCs can be written as follows.

$$V_{g2} = V_{g1} + R_{g1}I_{g1} - R_{g2}I_{g2} \tag{22}$$

$$K_2 I_{g2} - K_1 I_{g1} = R_{g1}I_{g1} - R_{g2}I_{g2} \tag{23}$$

The power-sharing ratio between GSC1 and GSC2 can be written as follows.

$$\frac{P_{g1}}{P_{g2}} = \frac{I_{g1}}{I_{g2}} = \frac{R_{g2} + K_2}{R_{g1} + K_1} = r \tag{24}$$

The droop gains of the two GSCs can be computed based on the assigned power-sharing ratio as follows.

$$\begin{aligned} K_1 &= \frac{1}{r}\left[\left(R_{g2} + K_2\right) - rR_{g1}\right] \\ K_2 &= r\left[\left(R_{g1} + K_1\right) - \frac{1}{r}R_{g2}\right] \end{aligned} \tag{25}$$

The ratio, r, can be permanent for a fixed droop gain operation. The adjustment of the ratio requires communication among the AC grids for the power-sharing rearrangement agreement. Also, to vary the power flow at the GSCs side, the droop constant can remain constant on one of the GSCs while it changes at the other one based on the desired power-sharing ratio. The RPD control's possible operational issues are similar to the FRD control due to the droop gains' static nature in both control schemes during the MTDC system operation. However, additional issues can be encountered due to the power-sharing ratio's update requirement [33], [62]. Such issues are the communication requisite, complication in analytic expression with MTDC network expansion, instability with ratio variations, and ratio uncertainty with unforced system variations (e.g., DC transmission line resistances).

Type 3: Sub-Optimal Minimum Transmission Loss-Based Droop (Sub-Optimal MTLD) Control

The transmission loss minimization in an MTDC network can be achieved by the OPF calculator at the secondary control layer. Nevertheless, this idea has been expanded to radial MTDC network structures with the operation of solely the decentralized control layer by deploying the DC voltage droop control with proper droop gain turning. As long as the power-sharing among the GSCs is inversely proportional to their respective DC transmission line resistances, the condition of minimum power transfer is achieved (under static MTDC system operation), as shown in (26) for two GSCs [49], [63].

$$\frac{P_{g1}}{P_{g2}} = \frac{I_{g1}}{I_{g2}} = \frac{R_{g2}}{R_{g1}} = \frac{K_2}{K_1} \tag{26}$$

This expression can be easily expanded for multiple GSCs in a large radial MTDC system [21], [30], [31]. However, under the unforced system moderate variations (i.e., DC transmission lines uncertainty and/or power injection variations), the tuned droop gains will achieve sub-optimal power flow. A communication interface with the secondary control layer will be required to update the droop gains and achieve the OPF for minimum power loss under system disturbance. The fixed droop gain for sub-optimal MTLD control for a radial MTDC can be obtained as follows.

$$K_j = \left[(I_g R_g) - V_{gL}\right]\left[I_T R_{gj}^T R_g\right]^T \tag{27}$$

$$I_g = \sum_{a=1}^{n} \frac{V_{ga}}{R_{ga}};\ R_g = \left(\sum_{a=1}^{n} R_{ga}^T\right)^T \tag{28}$$

This droop gain design allows the GSC with less distance from the WSCs to share more power compared to the other GSCs.

The fixed droop control design under system disturbances needs careful consideration [60], [64]. In the next section, the adaptive droop control has been introduced with local adjustable droop gains.

2) ADAPTIVE DROOP CONTROL (VARIABLE GAIN)

To accommodate the different operating conditions of the MTDC system, the adaptive DC voltage droop control has been introduced with a variable droop gain in an autonomous decentralized mode (i.e., without/or with reduced communication interface requirement). The outer and inner controller structure of a VSC with the DC voltage droop control is represented in Fig. 9, considering both the fixed and adaptive droop gain approaches.

With the adaptive droop gain, it is expected to have variations on the converter occupancy through the time in an MTDC system due to the power injection fluctuations and/or system disturbances. Consequently, the power-sharing at the

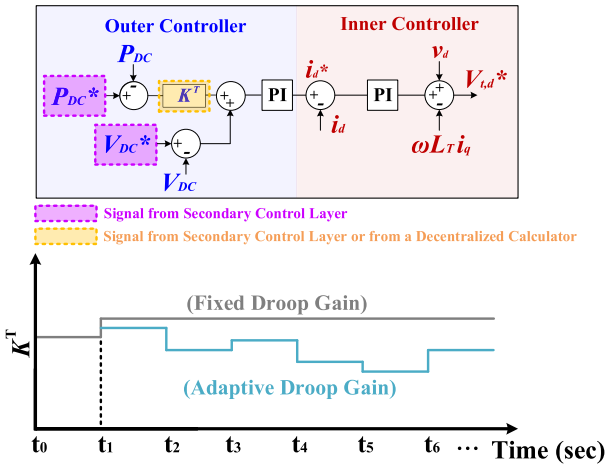

FIGURE 9. The outer and inner controller structure for a VSC with fixed or adaptive DC voltage droop control, where the DC voltage and power can be the GSC terminal DC signals.

GSCs will have continuous variations based on the adjusted droop gains. The droop gains tuning can impact the utilization of the converters' capacity, the DC voltages deviation, and the onshore AC grids frequency, which need to be limited within the constraints. The following adaptive droop gain tuning types have been introduced for converter capacity utilization.

Type 1: Available Headroom-Based Droop (AHD) Control

In the case of a converter operating near its active power limits, it is preferred to reduce its power-sharing not to hit the limits. The AHD control can achieve this through appropriate droop gain turning while respecting the Available Headroom (AH) of the converters. The AH of the j^{th} GSC can be expressed, as shown in (29).

$$AH_j^{(t)} = P_{gj,r} - P_{gj}^{(t-1)} \tag{29}$$

where $P_{gj}^{(t-1)}$ is the power occupied by the j^{th} GSC before the disturbance.

The converters of a higher AH will share more power compared to the converters of a lower AH to avoid control mode change from DC voltage droop control mode to constant power control mode. To achieve the AHD control, it is required to have an inverse proportional relationship between the droop gain and the AH of the respective converter. Several mathematical expressions have been presented in the literature to achieve this relationship for the AHD control [51], [56], [60], [64]. As have been pointed out in [60], the works [51], [56], and [64] attains the required relationship for AHD control for a single-disturbance event. However, with continuous/consecutive power disturbances, the presented AHD control methods do not consider the converter power limits. A droop gain perturbation technique has been presented in [60] for AHD control, such that considering the adaptive droop gain design during continuous power disturbances for constrained MTDC system operation, with the droop gain design presented in (30).

$$K_j^{(t)} = \left(K_j^{(t_0)} \frac{MR}{AH_j^{(t)}}\right)^{\alpha} + \Delta K_j^{(t)} \tag{30}$$

where $\Delta K_j^{(t)}$ is the perturbation factor based on [60]. $\alpha = 0.5$ for smooth droop gain transition.

Another study has taken into consideration the reactive power capacity of the converters, in addition to the active power, for the AHD control (i.e., unified AHD control for single-disturbance event), as presented in [65].

Type 2: Loading Factor-Based Droop (LFD) Control

The LFD control goal is to reduce the loading stress on the converters, which is of a similar objective to the AHD control. In this control type, the term Loading Factor (LF) is introduced to tune the droop gains based on the converters' loading capability. For the j^{th} GSC, the LF can be expressed as follows.

$$LF_j = \frac{P_{gj}}{P_{gj,r}} \times 100\% \tag{31}$$

This control method allows to adaptively control the power-sharing among the GSCs based on the LF, such that the GSC with the lowest LF will have the highest participation in the power-sharing. This concept has been presented in [60], for consecutive power disturbances, with a mathematical expression, as shown in (32), in addition to a droop gain perturbation technique. Further details are available in [60].

$$K_j^{(t)} = K_j^{(t_0)} \gamma_j \sum_{a=1}^{3} \frac{\left(P_{gj}^{(t-1)}\right)^a}{\frac{1}{2} P_{gj,r}{}^a} \tag{32}$$

where $\gamma_j = \dfrac{s \neq j}{\sum_{s=1}^{n} \left(P_{gs,r} + P_{gs}^{(t-1)}\right)}$ for n GSCs.

The centralized-based DC voltage droop control can also achieve the aforementioned droop control objectives; however, with a fast communication-link necessity between the secondary control layer and the decentralized control layers.

The DC voltage deviation is an essential factor for DC-side stability. Therefore, some studies have presented the adaptive droop gain design for the objective of DC voltage deviation minimization during the MTDC system disturbances [64], [66]. While for the AC-side stability consideration, the adaptive droop gains design for frequency margin control has been covered in some studies [56], [57], [67].

The adaptive droop gain can satisfy both the power and voltage constraints of the MTDC systems for any post-contingency operation with proper droop gain tuning. However, it is essential to highlight the prominence of the MTDC control system's stability analysis, which is out of the paper's scope.

V. CASE STUDIES: RESULTS AND DISCUSSION

In this section, case studies are presented for the DC voltage control methods covered in the previous sections. First,

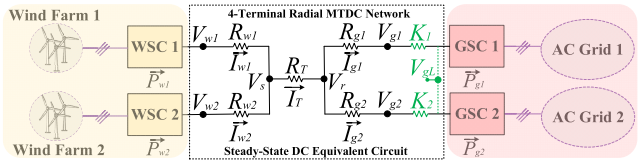

FIGURE 10. A 4-terminal radial MTDC network with its equivalent DC circuit representation in a steady-state condition.

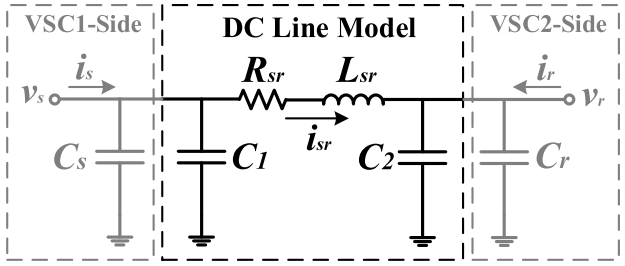

FIGURE 11. π-section DC equivalent circuit for an HVDC transmission line.

the MTDC system modeling is covered, then the case studies result and discussion are presented.

A. SYSTEM MODELING

1) CONVERTER MODELING

A 4-terminal radial MTDC network, 400 kV DC-link voltage, is used to apply the DC voltage control methods, as shown in Fig. 10. The network consists of two WSCs connected to wind farms and two GSCs connected to AC grids. The WSCs supply the AC grids with the maximum available power through the radial MTDC interconnection.

2) DC LINE MODELING

The HVDC transmission lines can be represented by a π-section equivalent model [23], [68], [69], as shown in Fig. 11. The terminal voltages' dynamics and the current through the series impedance for the π-section in Fig. 11 are represented by (33).

$$\begin{aligned} \dot{v_s} &= {C_{eq1}}^T(i_s - i_{sr}) \\ \dot{v_r} &= {C_{eq2}}^T(i_{sr} + i_r) \\ \dot{i_{sr}} &= {L_{sr}}^T(-R_{sr}i_{sr} + v_s - v_r) \end{aligned} \tag{33}$$

where $C_{eq1} = C_1 + C_s$ and $C_{eq2} = C_2 + C_r$.

The results section's focus will be on the steady-state behavior of the MTDC system with the different DC voltage control approaches.

3) SYSTEM PARAMETERS AND CONSTRAINTS

The DC line data and system rating of the radial MTDC network in Fig. 10 are available in [60]. The main system parameters are presented in TABLE 3.

The network's DC voltage constraint is as follows.

$$380 \text{ kV} \leq V_{DC} \leq 420 \text{ kV} \forall \text{ Nodes} \tag{34}$$

TABLE 3. Parameters of the 4-terminal radial MTDC network.

Parameter		Value
DC Line Resistance	R_{w1}	1 Ω
	R_{w2}	1.5 Ω
	R_T	2 Ω
	R_{g1}	1.2 Ω
	R_{g2}	0.8 Ω
WSC Power Rating	$P_{w1,r}$	500 MW
	$P_{w2,r}$	500 MW
GSC Power Rating	$P_{g1,r}$	300 MW
	$P_{g2,r}$	500 MW
DC-Link Voltage	V_{gL}	400 kV

where V_{DC} is a DC voltage node in the radial MTDC system, such that 380 kV refers to 0.95 pu while 420 kV refers to 1.05 pu.

The converters' power constraints are as follows.

$$\begin{aligned} -500\,MW &\leq P_{w1} \leq 0 \\ -500\,MW &\leq P_{w2} \leq 0 \\ 0 &\leq P_{g1} \leq 300 \text{ MW} \\ 0 &\leq P_{g2} \leq 500\,MW \end{aligned} \tag{35}$$

The converters' current constraints are as follows.

$$\begin{aligned} -1250 \text{ A} &\leq I_{w1} \leq 0 \\ -1250 \text{ A} &\leq I_{w2} \leq 0 \\ 0 &\leq I_{g1} \leq 750 \text{ A} \\ 0 &\leq I_{g2} \leq 1250 \text{ A} \end{aligned} \tag{36}$$

While the constraint of the line current flow, I_L, is as follows.

$$0 \leq I_L \leq 2500 \text{ A} \; \forall \text{ lines} \tag{37}$$

4) NORMAL AND ABNORMAL SYSTEM OPERATION

The power injection by the WSCs may fluctuate due to the nature of the RESs. Therefore, the MTDC system needs to adjust the power flow based on unexpected power variations. In this section, the presented case studies consider both the normal system operating (i.e., fixed power injection) and abnormal system operating (i.e., power injection variations) conditions.

To obtain and maintain efficient power transfer in the radial MTDC network, Fig. 10, it is possible to operate the system at the highest allowed DC voltage level with the condition presented in (38) [21].

$$\begin{aligned} V_{wp} &= 1.05 \; \forall t \forall P_{inj} \text{ s.t.} \\ \min(V_s) &= V_{wp} - \max(I_{wp}R_{wp}) \text{ and} \\ 0.95 \text{ pu} \leq V_{wi} &\leq 1.05 \text{ pu} \; \forall \quad i = 1, 2, \ldots, m. \end{aligned} \tag{38}$$

where V_{wp}, I_{wp}, and R_{wp} are the DC voltage, current, and line resistance of the WSC p that has the highest line voltage drop compared to the rest of the WSCs. P_{inj} is the total power injected by the WSCs as follows.

$$P_{inj} = P_{w1} + P_{w2} \tag{39}$$

In the following sections, the conventional and non-conventional DC voltage methods are applied for the radial MTDC network, Fig. 10, considering: (1) constant power injection by the WSCs (i.e., normal network operation) and (2) considering power input variations by the WSCs (i.e., abnormal network operation). The MTDC system operates at normal operating conditions between 0 sec to 1 sec, while the system operates in abnormal operating conditions between 1 sec to 13 sec with consecutive power disturbances.

B. CASE 1: CONVENTIONAL METHODS (NON-DROOP CONTROL BASED)

The results of Case 1 entail the following conventional DC voltage droop control method: M/S control (Scenario 1.1), TSO control (Scenario 1.2), and FDCT control (Scenario 1.3).

1) SCENARIO 1.1: M/S CONTROL

In this scenario, the master/slave control is applied for the DC voltage control of the radial MTDC network, Fig. 10. The WSC2 operates as the master converter (i.e., DC voltage control mode). While WSC1, GSC1, and GSC2 operate as slave converters (i.e., constant power control mode). The known variables, $\boldsymbol{NV}$, and unknown variables, $\boldsymbol{UV}$, for the DC load flow of the system are as follows. The input of the load flow is $\boldsymbol{NV} = \{P_{w1}, P_{g1}, P_{g2}, V_{ini}\}$. V_{ini} is the initial value of the network's DC voltages with the assumption $V_{ini} = 1.05$ pu (i.e., $V_{ini} = 420$ kV) for all the nodes, and this assumption is considered for all the upcoming scenarios. While the output of the load flow is $\boldsymbol{UV} = \{P_{w2}, V_{w1}, V_{w2}, V_s, V_r, V_{g1}, V_{g2}\}$. The results of Scenario 1.1 are presented in Fig. 12.

Fig. 12(a) shows the system operation during normal network operation, which shows constrained load flow. While Fig. 12(b)-(d) show the system behavior during consecutive power disturbances. The total power injection from the WSCs is approximately between 300 MW and 550 MW. The converters' power rating and DC voltages are within the allowed operating range. It can be seen that when WSC1 produces a power less than the required amount by the GSCs, then the master converter, WSC2, adjusts its power injection based on the requirement from the AC grids, as shown in Fig. 12(b) while preserving its DC voltage, V_{w2}, within the allowed operating range. The total power losses due to the DC transmission lines resistances are presented in Fig. 12(d), which is based on (8).

2) SCENARIO 1.2: TSO CONTROL (OPTIMAL POWER FLOW)

This scenario considers adjusting the OPF in the MTDC system for minimum transmission losses. The WSCs act in constant power control mode while the GSCs operate in DC voltage control mode, such that the DC voltages' references are updated regularly by the secondary control layer. The voltage reference update occurs in the incidence of input power disturbance with the optimization objective presented

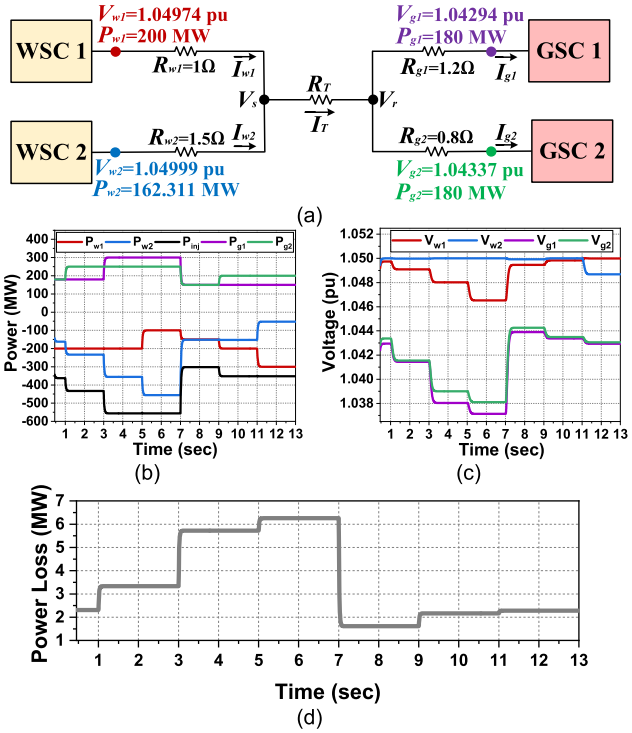

FIGURE 12. The voltage and power results of the M/S control (i.e., Scenario 1.1) (a) During normal network operation (b)-(c) During abnormal network operation (i.e., consecutive power disturbances) and (d) Transmission power losses during abnormal network operation.

in (3) and (8). Also, the optimization constraints are presented in (7) and (9)-(13). The Matlab Optimization Toolbox, in particular *fmincon*, has been applied for the optimization process, as elaborated further in [21]. Moreover, to obtain efficient power flow, the WSC2's terminal DC voltage is assigned to 1.05 pu, based on the condition presented in (38). In this scenario, the input of the network's load flow is $\boldsymbol{NV} = \{P_{w1}, P_{w2}, V_{w2}, V_{ini}\}$. While the output of the network's load flow is $\boldsymbol{UV} = \{V_{w1}, V_s, V_r, V_{g1}, V_{g2}\}$. The results of Scenario 1.2 are displayed in Fig. 13.

The MTDC system operation during normal operation is presented in Fig. 13(a), which shows constrained power flow with equivalent GSCs' terminal DC voltage, $V_{g1} = V_{g2}$, (i.e, the condition of transmission loss minimization is achieved [21], [30], [49]). The GSC with less transmission line resistance shares more power compared to other GSCs, for transmission loss minimization. In this case, based on the aforementioned condition, the GSC2 shares more power compared to GSC1. In the event of consecutive power disturbances, as presented in Fig. 13(b)-(d), the GSCs' terminal DC voltage remains equivalent at all times, as shown in Fig. 13(c), while the GSC2 continuously has the highest share of power, as displayed in Fig. 13(b). The total power injection from the WSCs is between 400 MW and 700 MW. The WSC2's terminal DC voltage remains operating at 1.05 pu, through all the times, for efficient power transfer. Overall, the results of the OPF are within the grid's limits.

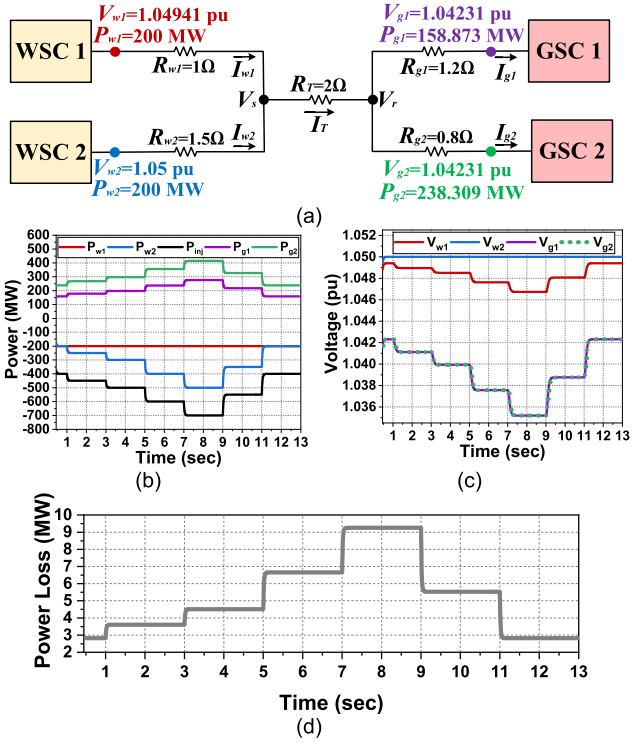

FIGURE 13. The voltage and power results of the TSO control (i.e., Scenario 1.2) (a) During normal network operation (b)-(c) During abnormal network operation (i.e., consecutive power disturbances) and (d) Transmission power losses during abnormal network operation.

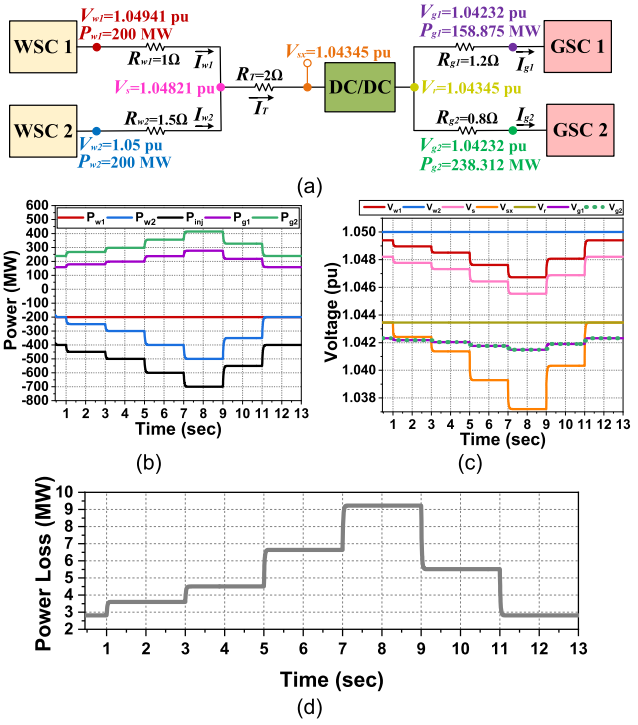

FIGURE 14. The voltage and power results of the FDCT control (i.e., Scenario 1.3) (a) During normal network operation (b)-(c) During abnormal network operation (i.e., consecutive power disturbances) and (d) Transmission power losses during abnormal network operation.

3) SCENARIO 1.3: FDCT CONTROL (DC VOLTAGE ENHANCEMENT)

In the aforementioned scenarios (Scenario 1.1 and Scenario 1.2), the power flow in the MTDC system is controlled by the WSCs and GSCs. Meanwhile, the power flow through the DC lines' interconnection depends solely on the lines' resistances. The power flow control in the DC lines requires incorporating an additional element, such as a high-power DC-DC converter, as in FDCT control. In this scenario, the high-power DC-DC converter is introduced at the longest DC transmission line of the radial MTDC network, Fig. 10, for DC voltage enhancement at the GSCs-side. Besides, this scenario considers the OPF (i.e., transmission loss minimization) and efficient power transfer conditions, similarly to Scenario 1.2.

The modified radial MTDC network with a lossless high-power DC-DC converter, during normal network operation, is presented in Fig. 14(a). The known and unknown variables for the load flow are as follows. $\boldsymbol{NV} = \{P_{w1}, P_{w2}, V_{w2}, V_r, V_{ini}\}$. $\boldsymbol{UV} = \{V_{w1}, V_s, V_{sx}, V_{g1}, V_{g2}\}$. Where V_{sx} and V_r are the input and output voltages of the DC-DC converter, respectively. Based on the condition presented in (14), the output of the DC-DC converter, V_r, is supposed to be enhanced to 420 kV. The results of Scenario 1.3 are shown in Fig. 14. While the base values for the power, voltage, current, and DC line's resistance are presented in TABLE 4. Further information about the base values calculations with high-power DC-DC converter incorporation in a radial MTDC network is available in [21].

TABLE 4. Base values of the modified radial MTDC network (Fig. 14(a)).

Parameter	$V_{base,1}$	$R_{base,1}$	$I_{base,1}$	P_{base}
Value	400 kV	320 Ω	1250 A	500 MW
Parameter	$V_{base,2}$	$R_{base,2}$	$I_{base,2}$	
Value	402.511 kV	324.029 Ω	1242.204 A	

Where $V_{base,1}$, $R_{base,1}$, and $I_{base,1}$ are the base voltage, resistance, and current for the input-side of the DC-DC converter. $V_{base,2}$, $R_{base,2}$, and $I_{base,2}$ are the base voltage, resistance, and current for the output-side of the DC-DC converter. P_{base} is the base power of the MTDC system.

As shown in Fig. 14(a), the power injection from the WSCs is the same profile as in Scenario 1.2. It can be seen from Fig. 14(c) that the output of the DC-DC converter is maintained at 1.04345 pu, that is 420 kV based on $V_{base,2}$, through all the consecutive power disturbances. While the GSCs' terminal DC voltages are equivalent for minimum transmission losses. The power losses presented in Fig. 14(d) are based on the following expression.

$$P_{TL} = \left(\sum_{i=1}^{2} (V_{wi} - V_s)^2 G_{wi}\right) + (V_s - V_{sx})^2 G_T + \left(\sum_{j=1}^{2} (V_r - V_{gj})^2 G_{gj}\right) \quad (40)$$

It can be seen that the GSCs' terminal DC voltages have been improved compared to Scenario 1.2 due to the inte-

gration of the high-power DC-DC converter. For example, during normal network operation, the GSCs' DC voltages are 419.546 kV in Scenario 1.3, while they are 416.923 kV in Scenario 1.2.

In Scenario 1.3, the MTDC system operates within the allowed voltage, current, and power operating ranges.

C. CASE 2: NON-CONVENTIONAL METHODS (DROOP CONTROL-BASED)

In the second case, the results of the following DC voltage droop control methods are presented and discussed: FRD control (Scenario 2.1), RPD control (Scenario 2.2), Sub-optimal MTLD control (Scenario 2.3), MTLD control (Scenario 2.4), AHD control (Scenario 2.5), and LFD control (Scenario 2.6). In all the subsequent scenarios, the WSCs act in the constant power control mode, whereas the GSCs operate in the DC voltage droop control mode. The power distribution among the GSCs depends on the assigned droop gains.

1) SCENARIO 2.1: FRD CONTROL (FIXED GAIN)

In this scenario, the droop gains are designed for the objective of power-sharing among the GSCs based on the GSCs' power rating (i.e., the GSC with the highest power rating will share more power compared to the lowest rated GSC). The droop function presented in (19) is used to acquire the droop gains while considering $H_j = P_{gj,r} \forall j$ (i.e., assuming $RP_j = 0$ in (20)). The initial droop gain, $K_j^{(t_0)}$, is assumed 5 $\Omega \forall j$, and the operation of the radial system based on this adjustment is presented in Fig. 15(a). To achieve the FRD control, based on (19) and (20), the droop gains are adjusted to $K_1^{(t)} = 8.333\ \Omega$ and $K_2^{(t)} = 3\Omega \forall t \neq 0$ sec (i.e., for 1sec $\leq t \leq$ 13sec).

In this scenario, $\boldsymbol{NV} = \left\{P_{w1}, P_{w2}, V_{ini}, K_1^{(t)}, K_2^{(t)}, \boldsymbol{K_{ini}}\right\}$ and $\boldsymbol{UV} = \left\{V_{w1}, V_{w2}, V_s, V_r, V_{g1}, V_{g2}\right\}$. Where $\boldsymbol{K_{ini}} = \left\{K_1^{(t_0)}, K_2^{(t_0)}\right\}$ is the initial droop gains. The total power injected by the WSCs, P_{inj}, is in the range between 400 MW and 700 MW, and the same power injection profile is considered for all the succeeding scenarios.

The results of the network, during normal and abnormal operation, with FRD control, are presented in Fig. 15. The normal operation result considers the adjustment of the droop gains to the initial value. While in the case of consecutive power disturbances, as shown in Fig. 15(b)-(d), the power change in GSC2 is higher than the changes in GSC1. Since the rating of GSC2 is 500 MW while the rating of GSC1 is 300 MW, as presented in TABLE 3, therefore, the droop gain of GSC2 is lower than GSC1, $K_2^{(t)} < K_1^{(t)}$ (i.e., GSC2 is allowed to take more power compared to GSC1). During the maximum power injection from the WSCs (i.e., 7 sec $\leq t <$ 9 sec), the GSC2 is almost fully loaded and operating near its maximum power rating. In general, the radial MTDC network operates within its limits, as presented in Fig. 15, and the transmission losses in this scenario are presented in Fig. 15(d).

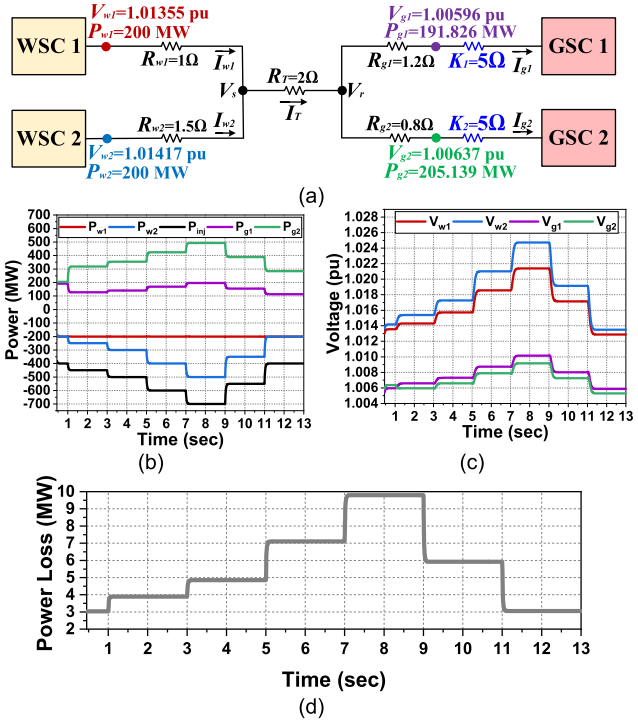

FIGURE 15. The voltage and power results of the FRD control (i.e., Scenario 2.1) (a) During normal network operation (b)-(c) During abnormal network operation (i.e., consecutive power disturbances) and (d) Transmission power losses during abnormal network operation.

2) SCENARIO 2.2: RPD CONTROL (FIXED GAIN)

This scenario considers the droop gain design with a predefined power-sharing ratio among the GSCs. The ratio gives priority to particular GSCs in terms of power participation. In a radial MTDC network with two GSCs, the droop gains design is based on solving the two equations in (25) for the droop gains. The presumed ratio, r, among the GSCs is to allow GSC1 with 30% power participation compared to GSC2 (i.e., $P_{g1} = 30\% P_{g2}$). Therefore, based on (24), the ratio, r, is taken as 0.3. The obtained droop gains for the GSCs is as follows, $K_1^{(t)} = 2.667\Omega$ and $K_2^{(t)} = 0.36\Omega \forall t$. The following is considered: $\boldsymbol{NV} = \left\{P_{w1}, P_{w2}, V_{ini}, K_1^{(t)}, K_2^{(t)}, r\right\}$ and $\boldsymbol{UV} = \left\{V_{w1}, V_{w2}, V_s, V_r, V_{g1}, V_{g2}\right\}$.

The results of the system during normal operation are presented in Fig. 16(a). It can be seen that GSC1 receives only 30% of the power received by the GSC2. Meanwhile, as shown in Fig. 16(b)-(d), the GSC1 and GSC2 continuously receive the power based on the specified ratio during the consecutive power disturbances during the abnormal network operation. It can be seen that during the maximum power injection from the GSCs, the GSC2 exceeds its power rating limit, as shown in Fig. 16(b) at 7 sec $\leq t <$ 9 sec. This is due to the fixed droop gain nature of the RPD control, such that it does not consider the GSCs' rating. The DC voltages of the network are within the permitted limits, and the transmission power losses of the radial network are presented in Fig. 16(d).

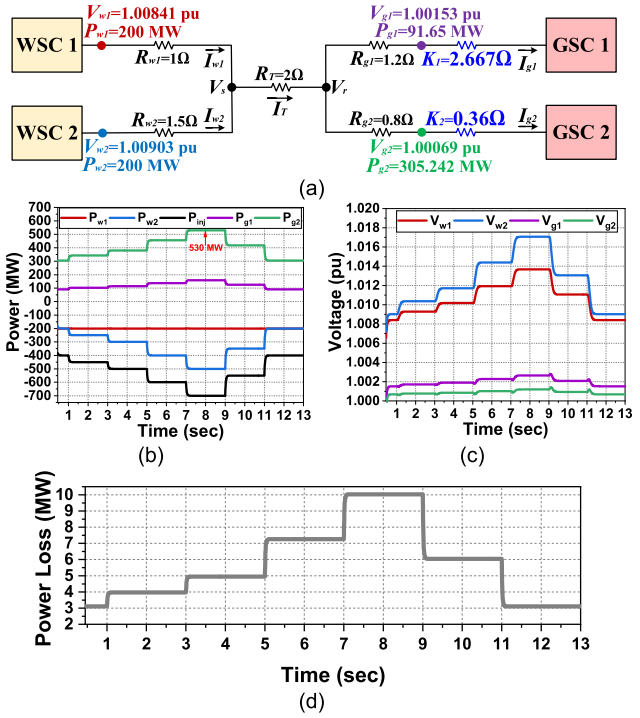

FIGURE 16. The voltage and power results of the RPD control (i.e., Scenario 2.2) (a) During normal network operation (b)-(c) During abnormal network operation (i.e., consecutive power disturbances) and (d) Transmission power losses during abnormal network operation.

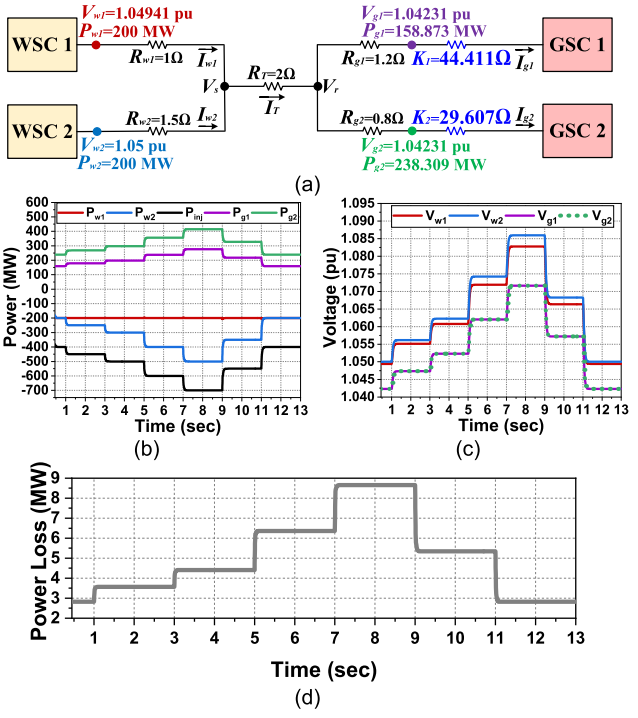

FIGURE 17. The voltage and power results of the Sub-Optimal MTLD control (i.e., Scenario 2.3) (a) During normal network operation (b)-(c) During abnormal network operation (i.e., consecutive power disturbances) and (d) Transmission power losses during abnormal network operation.

3) SCENARIO 2.3: SUB-OPTIMAL MTLD CONTROL (FIXED GAIN)

To achieve minimum transmission losses in a radial MTDC, the droop gains need to be inversely proportional to their respective GSC's current and power flow. The droop gains in this scenario are designed based on (26)-(28), which can be rewritten as follows for two GSCs [30], [49].

$$I_{g1} = \frac{R_{g2}}{R_{g1} + R_{g2}} I_T$$
$$\text{and } I_{g2} = \frac{R_{g1}}{R_{g1} + R_{g2}} I_T \tag{41}$$

The droop gains for minimum power losses can be computed by (15), (18), and (41). The droop gains are derived as follows. The resultant droop gains are $K_1^{(t)} = 44.411\Omega$ and $K_2^{(t)} = 29.607\Omega \forall t$, this is while considering the following operating-point: $V_{w2} = 1.05$ pu, $P_{w1} = 200$ MW, and $P_{w2} = 200$ MW (i.e., considering the minimum total power injection). Accordingly, the total current injected by the WSCs, I_T, is 952.7 A. This design operating-point is considered for the system during normal network operation, as presented in Fig. 17(a). It can be seen that the system operates within its allowed limits.

In the case of consecutive power disturbances, abnormal network operation, with the same droop gains setting $\forall t$ (i.e., fixed gains), the $\boldsymbol{NV}$ and $\boldsymbol{UV}$ are as follows.

$$\boldsymbol{NV} = \left\{P_{w1}, P_{w2}, V_{ini}, K_1^{(t)}, K_2^{(t)}\right\}.$$

$$\boldsymbol{UV} = \left\{V_{w1}, V_{w2}, V_s, V_r, V_{g1}, V_{g2}\right\}.$$

The results of the abnormal operation are presented in Fig. 17(b)-(d). The GSCs' received power is within the allowed rating; however, during 1 sec $\leq t <$ 11 sec, all the DC voltages of the network exceed the permitted limits above +5% of the network no-load voltage. It can be seen from Fig. 17(c) that the terminal DC voltage of WSC2 reaches a maximum of 1.0859 pu (i.e., 434.377 kV), and this may lead to infrastructure damage. In this scenario, the droop gains maintain OPF for the design operating-point, while they maintain sub-optimal power flow in the case of deviating from the design operating-point. The GSCs' DC voltages are equivalent during all the times due to sub-optimal power flow. As shown in Fig. 17(d), the resulting transmission losses in this scenario are lower than those of Scenarios 2.1 and 2.2.

4) SCENARIO 2.4: MTLD CONTROL (ADAPTIVE GAIN)

To achieve OPF with minimum transmission losses, at all the times during the consecutive power disturbances, the droop gains must be updated at each disturbance event. In this scenario, the droop gains adjustment during the normal network operation is similar to Scenario 2.3, as shown in Fig. 18(a). Therefore, similar results are obtained in Fig. 18(a) and Fig. 18(a). However, in the case of abnormal network operation, the results of Scenario 2.4 are presented in Fig. 18(b)-(d). The droop gains update are based on

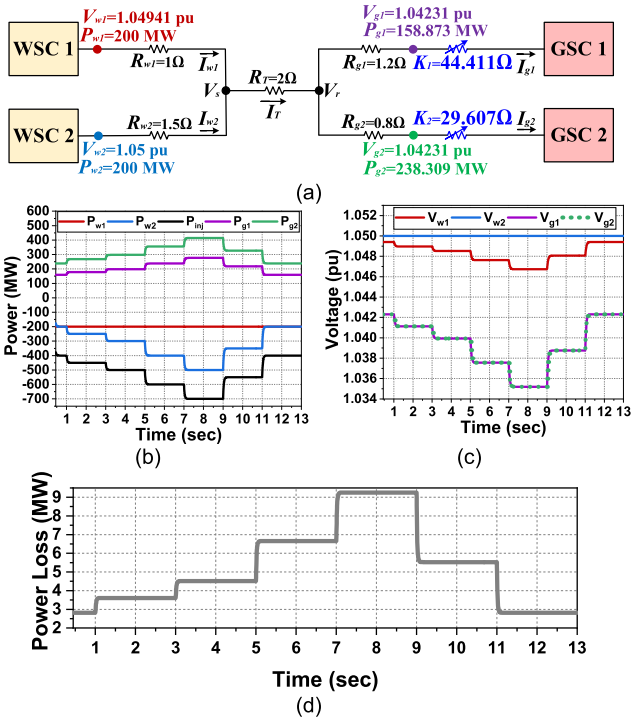

FIGURE 18. The voltage and power results of the MTLD control (i.e., Scenario 2.4) (a) During normal network operation (b)-(c) During abnormal network operation (i.e., consecutive power disturbances) and (d) Transmission power losses during abnormal network operation.

TABLE 5. Droop gains during abnormal operation for MTLD control (Scenario 2.4).

Time	t_0	t_1	t_3	t_5	t_7	t_9	t_{11}
K_1 (Ω)	44.41	38.36	33.53	26.28	21.1	29.57	44.41
K_2 (Ω)	29.61	25.58	22.35	17.52	14.06	19.71	29.61

Where t_i is the time of the occurrence of the power disturbance at the i^{th} sec.

TABLE 6. Droop gains and AH of the GSCs during abnormal operation for AHD control (Scenario 2.5).

Time	t_0	t_1	t_3	t_5	t_7	t_9	t_{11}
K_1 (Ω)	5	4.81	5.58	6.32	7.83	11.03	4.1
K_2 (Ω)	5	2.91	3.34	3.6	4.45	3.91	4.83
AH_1 (MW)	108.2	129.6	112.3	80.9	46.1	148.7	95.6
AH_2 (MW)	294.9	224.3	192.5	126.1	63.6	107.2	307.4

Where t_i is the time of the occurrence of the power disturbance at the i^{th} sec.

(15), (18), and (41) while achieving $V_{w2} = 1.05$ pu $\forall t$, and considering the WSCs' power injection profile. The ***NV*** and ***UV*** are similar to Scenario 2.3. The acquired droop gains during the consecutive power disturbances are presented in TABLE 5.

It can be seen that through all the times $K_1 > K_2$ (i.e., GSC2 shares more power compared to GSC1). Since the transmission line resistance of GSC1, R_{g1}, is higher than of GSC2, R_{g2}. Therefore, it is expected that less transmission losses occur in case less power is transmitted through the path with the highest line resistance.

TABLE 7. Droop gains and LF of the GSCs during abnormal operation for LFD control (Scenario 2.6).

Time	t_0	t_1	t_3	t_5	t_7	t_9	t_{11}
K_1 (Ω)	5	18.78	9.55	23.7	17.25	40.19	15.85
K_2 (Ω)	5	4.52	7.16	7.01	11.39	13.17	9.72
LF_1 (%)	63.9	31.3	70.3	47.2	91.6	45.8	50.5
LF_2 (%)	41	70.4	56.9	90.3	83.2	81.4	49.1

Where t_i is the time of the occurrence of the power disturbance at the i^{th} sec.

The results of the network operation during normal and abnormal operation, as shown in Fig. 18, are constrained within the permissible limits. In addition, in contrast to Scenario 2.3, due to the droop gains' adaptive nature, the DC voltages are within the ±5% of the system no-load voltage, as presented in Fig. 18(c). The transmission losses in this scenario, as displayed in Fig. 18(d), are less compared to scenarios 2.1 and 2.2. The MTLD control obtains OPF for minimum power losses with a similar outcome to TSO control (i.e., Scenario 1.2); however, in Scenario 2.4, the GSCs operate in DC voltage droop control with adaptive droop gain.

5) SCENARIO 2.5: AHD CONTROL (ADAPTIVE GAIN PERTURBATION)

This scenario presents the power-sharing among the GSCs based on the AH, (29), of the converters (i.e., the GSC with the highest AH at time t shares more power compared to the other GSCs at time $t+1$). The droop gains can be adjusted to achieve AHD control based on an adaptive gain perturbation technique, as presented in (30). The initial droop gain, $K_j^{(t_0)}$, is set to 5 Ω$\forall j$. The maximum power rating among the GSCs, MR, is 500 MW while $\alpha = 0.5$. In this scenario, the ***NV*** and ***UV*** are same as Scenario 2.3.

The result of the radial MTDC network, during normal operation, with the droop gains adjusted for the initial values, is presented in Fig. 19(a), which gives similar results to Fig. 15(a).

The radial network results during abnormal operation with the AHD control are presented in Fig. 19(b)-(d). In addition, the droop gains and the AH of the GSCs, during the consecutive power disturbances are shown in TABLE 6.

At the initial time, 0 sec $\leq t <$ 1 sec, the behavior of the AH is as follows: $AH_2^{(t_0)} > AH_1^{(t_0)}$. Therefore, at time t_1, the change in the received power by the GSC2 is higher than GSC1 (i.e., GSC2 has the highest power participation to reduce the burden over the converter with lower AH, GSC1). During the consecutive power disturbances, the AH of GSC2 remains higher than GSC1, as shown in TABLE 6, until the disturbance occurrence at time t_9. At time t_9 (i.e., 9 sec $\leq t <$ 11 sec), the AH of GSC1 becomes higher than GSC2. Therefore, at t_{11} (i.e., 11 sec $\leq t \leq$ 13 sec), the change

TABLE 8. Comprehensive comparison between the DC voltage control methods.

Method	VCM	CO	E	CV	CM	DC	CF	Refs
M/S Control	Direct Voltage Control	Power Flow Balance	Moderate	Not Possible	Required	Not Complex	Not Flexible	[6],[24],[26], [29],[32],[33]
VM Control		Power Flow Balance	Moderate	Not Possible	Required	Not Complex	Not Flexible	[24],[29],[33], [34]
TSO Control		Optimal Power Flow	High	Not Possible	Required	Not Complex	Flexible	[25],[33],[35], [36],[37]
FDCT Control		Efficient Network Operation or/and DC Voltage Level Matching	High	Not Possible	Required	Not Complex	Flexible	[19],[20],[21]
MTLD Control	Droop Gain Control	Minimum Power Losses	High	Not Possible	Required	Not Complex	Flexible	[30],[68]
TSOD Control		Minimum Power Losses	High	Not Possible	Required	Not Complex	Flexible	[12],[13],[14], [17],[48]
FRD Control		Rating-Based Power Distribution	Moderate	Possible	Not Required	Not Complex	Not Flexible	[51],[56],[60]
RPD Control		Ratio-Based Power Distribution	Moderate	Possible	Not Required	Complex	Not Flexible	[24],[33],[61], [62]
Sub-Optimal MTLD Control		Minimum Power Losses	High	Possible	Not Required	Not Complex	Not Flexible	[21],[30],[31], [49],[63]
AHD Control		AH-Based Power Distribution	Moderate	Not Possible	Required	Complex	Flexible	[51],[56],[60], [64]
LFD Control		LF-Based Power Distribution	Moderate	Not Possible	Required	Complex	Flexible	[60]

Where VCM: Voltage Control Method. CO: Control Objective. E: Efficiency. CV: Constraints Violation. CM: Communication. DC: Design Complexity. CF: Configuration Flexibility. Refs: References.

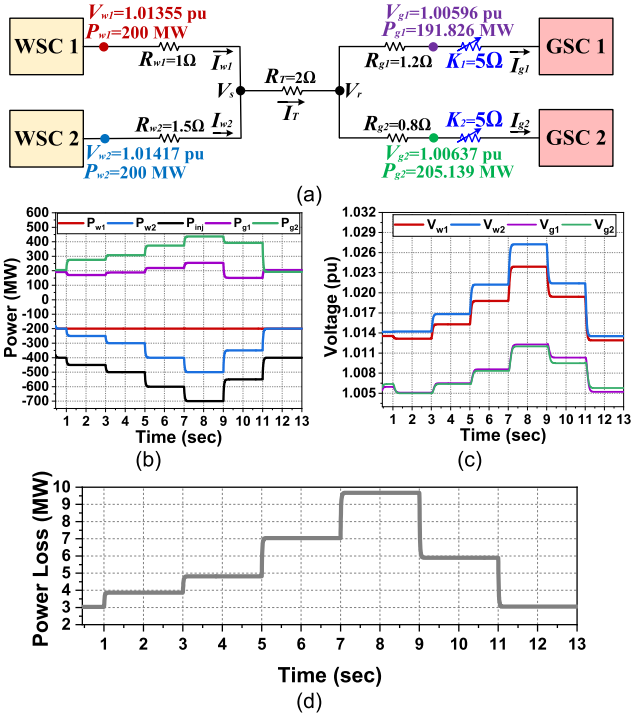

FIGURE 19. The voltage and power results of the AHD control (i.e., Scenario 2.5) (a) During normal network operation (b)-(c) During abnormal network operation (i.e., consecutive power disturbances) and (d) Transmission power losses during abnormal network operation.

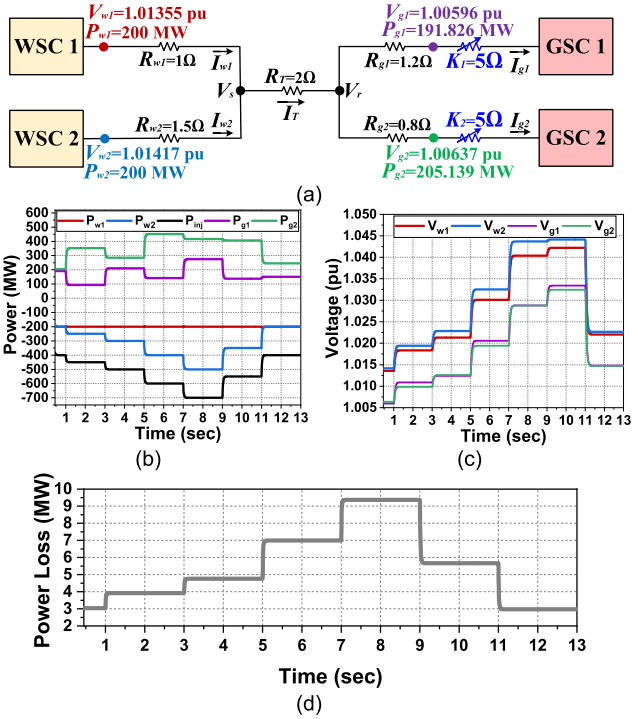

FIGURE 20. The voltage and power results of the LFD control (i.e., Scenario 2.6) (a) during normal network operation (b)-(c) during abnormal network operation (i.e., consecutive power disturbances) and (d) transmission power losses during abnormal network operation.

in the power received by GSC1 is higher than GSC2 (i.e., the power participation of GSC1 is increased to reduce the burden on GSC2). Overall, when the total injected power by the WSCs increases, the GSC with the highest AH at time t will have more change in the received power at time $t+1$, in a positive amount. Whereas when the total injected power by the WSCs decreases, the GSC with the lowest AH at time t will have the highest power change at time $t+1$, in a negative amount, to reduce the stress over the converter. Moreover, the radial network operates within its allowed limits. The

TABLE 9. Pros and cons of the DC voltage control methods.

Method	Advantage	Disadvantage
M/S Control	-Suitable for small-scale power fluctuation.	-Control reliability depends on a single converter. -Fast communication requirement. -Control of large-scale power disturbances limited to master converter rating.
VM Control	-Suitable for large-scale power fluctuation. -Back-up converter is available in case of a master converter outage.	-DC voltage swapping. -Fast communication requirement.
TSO Control	-Provide supplementary control actions (e.g., OPF). -Several converters share the role of DC voltage control.	-Regular update of the control set-points. -Fast communication requirement. -Optimization process complexity and time consumption.
FDCT Control	-Efficient power transfer. -Flexible power transfer. -Voltage and network configuration matching.	-Additional hardware complication and cost.
MTLD Control	-Transmission losses minimization at all times, including power disturbances. -Several converters share the role of DC voltage control.	-Multi-updated droop constant. -Fast communication requirement.
TSOD Control	-Power and voltage control via the droop constant. -Supplementary control actions (e.g., OPF). -Several converters share the role of DC voltage control.	-Multi-updated droop constant. -Fast communication requirement. -Optimization process complexity and time consumption.
FRD Control	-Power-sharing based on converters' rating. -Simple droop gain calculation for large-scale radial systems. -Single-updated droop gain calculation. -Reduced communication requirement. -Several converters share the role of DC voltage control.	-Possible converter overloading. -Possible DC voltage rating violation. -Complicated analytical expression for large-scale complex systems.
RPD Control	-Power-sharing priority among converters based on a ratio. -Single-updated or multi-updated ratio. -Several converters share the role of DC voltage control.	-Possible ratio update and communication requirement. -Complicated calculation expression for complex systems. -Ratio uncertainty due to system parameters uncertainty.
Sub-Optimal MTLD Control	-Transmission loss minimization. -Single-updated droop constant. -Reduced communication requirement. -Several converters share the role of DC voltage control.	-Possible network DC voltage rating violation. -Possible converter rating violation. -Droop gain sensitivity to forced/unforced system variations. -Droop constant design complication for a complex system.
AHD Control	-Power-sharing based on the AH of the converters. -Several converters share the role of DC voltage control.	-Multi-updated droop gain. -Fast communication requirement. -Complex analytical computation.
LFD Control	-Power-sharing based on the LF of the converters. -Several converters share the role of DC voltage control.	-Multi-updated droop gain. -Fast communication requirement. -Complex analytical computation.

transmission losses during the abnormal system operation are presented in Fig. 19(d).

6) SCENARIO 2.6: LFD CONTROL (ADAPTIVE GAIN)

In this scenario, the power-sharing among the GSCs is based on the loading capability of the GSCs (i.e., the GSC with the highest LF, (31), will have the least participation in the power delivery). In this case, the droop gains for LFD control are adjusted based on the function presented in (32). Similar to the previous scenario, the initial droop gains are taken as 5 Ω for all the GSCs. Also, the ***NV*** and ***UV*** are same as Scenario 2.3. The results of the radial MTDC operation with the initial droop gains adjustment are presented in Fig. 20(a), which is similar to the outcomes of Fig. 15(a) and Fig. 19(a).

The droop gains adjustment and the LF of the GSCs, during the abnormal operation, are presented in TABLE 7.

While the result of radial network operation with the LFD control is presented in Fig. 20(b)-(d). As shown in TABLE 7, the LF of the GSCs follows a zigzag behavior, such that at each disturbance event, if $LF_1 > LF_2$ then at the next disturbance event, the LF behavior becomes $LF_2 > LF_1$, and the reverse is true. In general, when the total power injected by the WSCs increases, the GSC with the lowest LF at time t will have more change in the received power at time $t + 1$, in a positive amount. Meanwhile, when the total power injected by the WSCs decreases, the GSC with the highest LF at time t will have the highest power change at time $t + 1$, in a negative amount, to reduce the stress over the converter.

Overall, the system operates within the permitted limits, as shown in Fig. 20, and the transmission losses of the network are displayed in Fig. 20(d).

VI. COMPREHENSIVE EVALUATION: APPLICATION IN THE MTDC SYSTEM

The aforementioned DC voltage control methods can be employed in an MTDC network based on the system requirement, network configuration, and available resources. A comparison among the presented DC voltage control methods is presented in TABLE 8 and TABLE 9. The comparison considers the following factors: DC voltage control objective, the DC transmission system efficiency, constraint violation of the DC system, communication requirement, the complexity of the DC voltage control method, configuration flexibility of the MTDC network, and the available research references.

VII. CONCLUSION

A. SUMMARY

In conclusion, this paper presented a comprehensive review of the DC voltage control methods in an MTDC system. The main factor for power flow balance in an MTDC network is the control of DC voltages. The DC voltage can be controlled locally with decentralized control techniques. Besides, it can be controlled globally via centralized control techniques. This paper delivered a general classification of the DC voltage control methods, as was presented in Fig. 1 in Section I. The control methods and their design approaches were delivered from the perspective of post-contingency stability. The main control methods were studied and simulated with a 400 kV radial MTDC network, considering both normal and abnormal network operating conditions. Moreover, a comparison among the control methods was presented, as presented in TABLE 8. The DC voltage control methods can be deployed based on the MTDC system configuration, communication accessibility, and the control objective requirement by the transmission system operator (e.g., minimum transmission losses, power distribution based on the converters' capabilities, efficient power transfer, a hybrid combination of the aforementioned objectives, or any other system requirement).

B. FUTURE WORK

The dynamic stability of the MTDC network is a vital aspect of a reliable system operation. Therefore, the presented DC voltage control approaches require dynamic stability analysis in the future. These approaches can also be assessed in parallel with the interline power flow controller and FDTC approaches (i.e., integrating a DC-DC converter) for optimal power flow and improved congestion management. Besides, these control methods can be tested with emergency system operation (e.g., full or partial converters disconnection and line outages).

ACKNOWLEDGMENT

The statements made herein are solely the responsibility of the authors.

REFERENCES

[1] S. R. Sinsel, R. L. Riemke, and V. H. Hoffmann, "Challenges and solution technologies for the integration of variable renewable energy sources—A review," *Renew. Energy*, vol. 145, pp. 2271–2285, Jan. 2020, doi: 10.1016/j.renene.2019.06.147.

[2] *Global Sustainable Development Report 2019: The Future is Now—Science for Achieving Sustainable Development*, UN, New York, NY, USA, 2019.

[3] J. Sun, M. Li, Z. Zhang, T. Xu, J. He, H. Wang, and G. Li, "Renewable energy transmission by HVDC across the continent: System challenges and opportunities," *CSEE J. Power Energy Syst.*, vol. 3, no. 4, pp. 353–364, Dec. 2017, doi: 10.17775/CSEEJPES.2017.01200.

[4] D. Zhou, M. H. Rahman, L. Xu, and Y. Wang, "Impact of DC protection strategy of large HVDC network on frequency response of the connected AC system," *J. Eng.*, vol. 2019, no. 17, pp. 4031–4035, Jun. 2019, doi: 10.1049/joe.2018.8150.

[5] D. Babazadeh, D. Van Hertem, and L. Nordström, "Study of centralized and distributed coordination of power injection in multi-TSO HVDC grid with large off-shore wind integration," *Electr. Power Syst. Res.*, vol. 136, pp. 281–288, Jul. 2016, doi: 10.1016/j.epsr.2016.03.001.

[6] W. Wang and M. Barnes, "Power flow algorithms for multi-terminal VSC-HVDC with droop control," *IEEE Trans. Power Syst.*, vol. 29, no. 4, pp. 1721–1730, Jul. 2014, doi: 10.1109/TPWRS.2013.2294198.

[7] E. Jiménez, M. J. Carrizosa, A. Benchaib, G. Damm, and F. Lamnabhi-Lagarrigue, "A new generalized power flow method for multi connected DC grids," *Int. J. Electr. Power Energy Syst.*, vol. 74, pp. 329–337, Jan. 2016, doi: 10.1016/j.ijepes.2015.07.032.

[8] S. Cole, J. Beerten, and R. Belmans, "Generalized dynamic VSC MTDC model for power system stability studies," *IEEE Trans. Power Syst.*, vol. 25, no. 3, pp. 1655–1662, Aug. 2010, doi: 10.1109/TPWRS.2010.2040846.

[9] J. Beerten, S. Cole, and R. Belmans, "Generalized steady-state VSC MTDC model for sequential AC/DC power flow algorithms," *IEEE Trans. Power Syst.*, vol. 27, no. 2, pp. 821–829, May 2012, doi: 10.1109/TPWRS.2011.2177867.

[10] A. Egea-Alvarez, J. Beerten, D. Van Hertem, and O. Gomis-Bellmunt, "Hierarchical power control of multiterminal HVDC grids," *Electr. Power Syst. Res.*, vol. 121, pp. 207–215, Apr. 2015, doi: 10.1016/j.epsr.2014.12.014.

[11] D. Kotur and P. Stefanov, "Optimal power flow control in the system with offshore wind power plants connected to the MTDC network," *Int. J. Electr. Power Energy Syst.*, vol. 105, pp. 142–150, Feb. 2019, doi: 10.1016/j.ijepes.2018.08.012.

[12] K. Rouzbehi, A. Miranian, A. Luna, and P. Rodriguez, "DC voltage control and power sharing in multiterminal DC grids based on optimal DC power flow and voltage-droop strategy," *IEEE J. Emerg. Sel. Topics Power Electron.*, vol. 2, no. 4, pp. 1171–1180, Dec. 2014, doi: 10.1109/JESTPE.2014.2338738.

[13] C. Gavriluta, I. Candela, A. Luna, A. Gomez-Exposito, and P. Rodriguez, "Hierarchical control of HV-MTDC systems with droop-based primary and OPF-based secondary," *IEEE Trans. Smart Grid*, vol. 6, no. 3, pp. 1502–1510, May 2015, doi: 10.1109/TSG.2014.2365854.

[14] M. Han, D. Xu, and L. Wan, "Hierarchical optimal power flow control for loss minimization in hybrid multi-terminal HVDC transmission system," *CSEE J. Power Energy Syst.*, vol. 2, no. 1, pp. 40–46, Mar. 2016, doi: 10.17775/CSEEJPES.2016.00007.

[15] C. Gavriluta, R. Caire, A. Gomez-Exposito, and N. Hadjsaid, "A distributed approach for OPF-based secondary control of MTDC systems," *IEEE Trans. Smart Grid*, vol. 9, no. 4, pp. 2843–2851, Jul. 2018, doi: 10.1109/TSG.2016.2621775.

[16] K. Meng, W. Zhang, Y. Li, Z. Y. Dong, Z. Xu, K. P. Wong, and Y. Zheng, "Hierarchical SCOPF considering wind energy integration through multiterminal VSC-HVDC grids," *IEEE Trans. Power Syst.*, vol. 32, no. 6, pp. 4211–4221, Nov. 2017, doi: 10.1109/TPWRS.2017.2679279.

[17] X. Li, L. Guo, C. Hong, Y. Zhang, Y. W. Li, and C. Wang, "Hierarchical control of multiterminal DC grids for large-scale renewable energy integration," *IEEE Trans. Sustain. Energy*, vol. 9, no. 3, pp. 1448–1457, Jul. 2018, doi: 10.1109/TSTE.2018.2789465.

[18] F. A. Chachar, S. S. H. Bukhari, F. H. Mangi, D. E. Macpherson, G. P. Harrison, W. Bukhsh, and J.-S. Ro, "Hierarchical control implementation for meshed AC/Multi-terminal DC grids with offshore windfarms integration," *IEEE Access*, vol. 7, pp. 142233–142245, 2019, doi: 10.1109/ACCESS.2019.2944718.

[19] A. Garces, D. Montoya, and R. Torres, "Optimal power flow in multi-terminal HVDC systems considering DC/DC converters," in *Proc. IEEE 25th Int. Symp. Ind. Electron. (ISIE)*, Jun. 2016, pp. 1212–1217, doi: 10.1109/ISIE.2016.7745067.

[20] K. Rouzbehi, J. I. Candela, A. Luna, G. B. Gharehpetian, and P. Rodriguez, "Flexible control of power flow in multiterminal DC grids using DC–DC converter," *IEEE J. Emerg. Sel. Topics Power Electron.*, vol. 4, no. 3, pp. 1135–1144, Sep. 2016, doi: 10.1109/JESTPE.2016.2574458.

[21] S. Sayed and A. Massoud, "Optimal power flow in multi-terminal HVDC networks with embedded high-power DC–DC converters for voltage matching and flexible DC transmission," *IET Gener., Transmiss. Distrib.*, vol. 14, no. 18, pp. 3866–3876, Sep. 2020, doi: 10.1049/iet-gtd.2019.1238.

[22] D. Babazadeh, A. Muthukrishnan, P. Mitra, T. Larsson, and L. Nordström, "Selection of DC voltage controlling station in an HVDC grid," *Electr. Power Syst. Res.*, vol. 144, pp. 224–232, Mar. 2017, doi: 10.1016/j.epsr.2016.12.008.

[23] S. Sayed and A. Massoud, "A MATLAB/simulink-based average-value model of multi-terminal HVDC network," in *Proc. 2nd Int. Conf. Smart Grid Renew. Energy (SGRE)*, Nov. 2019, pp. 1–6, doi: 10.1109/SGRE46976.2019.9021020.

[24] F. D. Bianchi, J. L. Domínguez-García, and O. Gomis-Bellmunt, "Control of multi-terminal HVDC networks towards wind power integration: A review," *Renew. Sustain. Energy Rev.*, vol. 55, pp. 1055–1068, Mar. 2016, doi: 10.1016/j.rser.2015.11.024.

[25] K. Sun, K.-J. Li, W.-J. Lee, Z.-D. Wang, W. Bao, Z. Liu, and M. Wang, "VSC-MTDC system integrating offshore wind farms based optimal distribution method for financial improvement on wind producers," *IEEE Trans. Ind. Appl.*, vol. 55, no. 3, pp. 2232–2240, May 2019, doi: 10.1109/TIA.2019.2897672.

[26] R. Teixeira Pinto, S. F. Rodrigues, P. Bauer, and J. Pierik, "Comparison of direct voltage control methods of multi-terminal DC (MTDC) networks through modular dynamic models," in *Proc. 14th Eur. Conf. Power Electron. Appl.*, Aug. 2011, pp. 1–10.

[27] L. Xu and L. Yao, "DC voltage control and power dispatch of a multi-terminal HVDC system for integrating large offshore wind farms," *IET Renew. Power Gener.*, vol. 5, no. 3, p. 223, 2011, doi: 10.1049/iet-rpg.2010.0118.

[28] O. D. Adeuyi, M. Cheah-Mane, J. Liang, L. Livermore, and Q. Mu, "Preventing DC over-voltage in multi-terminal HVDC transmission," *CSEE J. Power Energy Syst.*, vol. 1, no. 1, pp. 86–94, Mar. 2015, doi: 10.17775/CSEEJPES.2015.00011.

[29] T. K. Vrana, J. Beerten, R. Belmans, and O. B. Fosso, "A classification of DC node voltage control methods for HVDC grids," *Electr. Power Syst. Res.*, vol. 103, pp. 137–144, Oct. 2013, doi: 10.1016/j.epsr.2013.05.001.

[30] S. Sayed and A. Massoud, "Minimum transmission power loss in multi-terminal HVDC systems: A general methodology for radial and mesh networks," *Alexandria Eng. J.*, vol. 58, no. 1, pp. 115–125, Mar. 2019, doi: 10.1016/j.aej.2018.12.007.

[31] S. Sayed and A. Massoud, "Impact of forced and unforced system parameter variations on network stability and system economics of radial MTDC networks," *Electr. Power Syst. Res.*, vol. 179, Feb. 2020, Art. no. 106051, doi: 10.1016/j.epsr.2019.106051.

[32] W. Lu and B.-T. Ooi, "Optimal acquisition and aggregation of offshore wind power by multiterminal voltage-source HVDC," *IEEE Trans. Power Del.*, vol. 18, no. 1, pp. 201–206, Jan. 2003, doi: 10.1109/TPWRD.2002.803826.

[33] R. T. Pinto, P. Bauer, S. F. Rodrigues, E. J. Wiggelinkhuizen, J. Pierik, and B. Ferreira, "A novel distributed direct-voltage control strategy for grid integration of offshore wind energy systems through MTDC network," *IEEE Trans. Ind. Electron.*, vol. 60, no. 6, pp. 2429–2441, Jun. 2013, doi: 10.1109/TIE.2012.2216239.

[34] T. Nakajima and S. Irokawa, "A control system for HVDC transmission by voltage sourced converters," in *Proc. IEEE Power Eng. Soc. Summer Meeting. Conf.*, Jul. 1999, pp. 1113–1119, doi: 10.1109/PESS.1999.787474.

[35] S. Chondrogiannis and M. P. Blanco, "Market integration scheme of a multi-terminal HVDC grid in the north seas," *IEEE Trans. Power Syst.*, vol. 31, no. 3, pp. 2415–2422, May 2016, doi: 10.1109/TPWRS.2015.2465860.

[36] M. J. Carrizosa, F. D. Navas, G. Damm, and F. Lamnabhi-Lagarrigue, "Optimal power flow in multi-terminal HVDC grids with offshore wind farms and storage devices," *Int. J. Electr. Power Energy Syst.*, vol. 65, pp. 291–298, Feb. 2015, doi: 10.1016/j.ijepes.2014.10.016.

[37] M. Aragüés-Peñalba, A. Egea-Àlvarez, O. Gomis-Bellmunt, and A. Sumper, "Optimum voltage control for loss minimization in HVDC multi-terminal transmission systems for large offshore wind farms," *Electr. Power Syst. Res.*, vol. 89, pp. 54–63, Aug. 2012, doi: 10.1016/j.epsr.2012.02.006.

[38] S. E. De Leon-Aldaco, H. Calleja, and J. A. Alquicira, "Metaheuristic optimization methods applied to power converters: A review," *IEEE Trans. Power Electron.*, vol. 30, no. 12, pp. 6791–6803, Dec. 2015, doi: 10.1109/TPEL.2015.2397311.

[39] J. C. S. De Souza, M. B. Do Coutto Filho, and M. L. R. Roberto, "A genetic-based methodology for evaluating requested outages of power network elements," *IEEE Trans. Power Syst.*, vol. 26, no. 4, pp. 2442–2449, Nov. 2011, doi: 10.1109/TPWRS.2011.2138727.

[40] I. A. Farhat and M. E. El-Hawary, "Optimization methods applied for solving the short-term hydrothermal coordination problem," *Electr. Power Syst. Res.*, vol. 79, no. 9, pp. 1308–1320, Sep. 2009, doi: 10.1016/j.epsr.2009.04.001.

[41] M. Aragüés-Peñalba, A. Egea-Àlvarez, S. G. Arellano, and O. Gomis-Bellmunt, "Droop control for loss minimization in HVDC multi-terminal transmission systems for large offshore wind farms," *Electr. Power Syst. Res.*, vol. 112, pp. 48–55, Jul. 2014, doi: 10.1016/j.epsr.2014.03.013.

[42] X. Zhong, M. Zhu, Y. Li, S. Wang, H. Wang, and X. Cai, "Modular interline DC power flow controller," *IEEE Trans. Power Electron.*, vol. 35, no. 11, pp. 11707–11719, Nov. 2020, doi: 10.1109/TPEL.2020.2989197.

[43] B. K. Johnson, R. H. Lasseter, F. L. Alvarado, and R. Adapa, "Expandable multiterminal DC systems based on voltage droop," *IEEE Trans. Power Del.*, vol. 8, no. 4, pp. 1926–1932, 1993, doi: 10.1109/61.248304.

[44] Y. Liu, T. C. Green, J. Wu, K. Rouzbehi, A. Raza, and D. Xu, "A new droop coefficient design method for accurate power-sharing in VSC-MTDC systems," *IEEE Access*, vol. 7, pp. 47605–47614, 2019, doi: 10.1109/ACCESS.2019.2909044.

[45] K. Rouzbehi, A. Miranian, J. I. Candela, A. Luna, and P. Rodriguez, "A generalized voltage droop strategy for control of multiterminal DC grids," *IEEE Trans. Ind. Appl.*, vol. 51, no. 1, pp. 607–618, Jan. 2015, doi: 10.1109/TIA.2014.2332814.

[46] W. Wang, M. Barnes, and O. Marjanovic, "Stability limitation and analytical evaluation of voltage droop controllers for VSC MTDC," *CSEE J. Power Energy Syst.*, vol. 4, no. 2, pp. 238–249, Jun. 2018, doi: 10.17775/CSEEJPES.2016.00670.

[47] H. Li, C. Liu, G. Li, and R. Iravani, "An enhanced DC voltage droop-control for the VSC-HVDC grid," *IEEE Trans. Power Syst.*, vol. 32, no. 2, pp. 1520–1527, Mar. 2017, doi: 10.1109/TPWRS.2016.2576901.

[48] M. A. Abdelwahed and E. F. El-Saadany, "Power sharing control strategy of multiterminal VSC-HVDC transmission systems utilizing adaptive voltage droop," *IEEE Trans. Sustain. Energy*, vol. 8, no. 2, pp. 605–615, Apr. 2017, doi: 10.1109/TSTE.2016.2614223.

[49] A. S. Abdel-Khalik, A. M. Massoud, A. A. Elserougi, and S. Ahmed, "Optimum power transmission-based droop control design for multi-terminal HVDC of offshore wind farms," *IEEE Trans. Power Syst.*, vol. 28, no. 3, pp. 3401–3409, Aug. 2013, doi: 10.1109/TPWRS.2013.2238685.

[50] J. Zhu, F. Li, Y. Liu, G. P. Adam, M. Li, and N. Sun, "An intelligent implementation of fuzzy search based nonlinear droop control scheme for multi-terminal DC transmission systems," *IEEE Access*, vol. 7, pp. 185951–185960, 2019, doi: 10.1109/ACCESS.2019.2950819.

[51] N. R. Chaudhuri and B. Chaudhuri, "Adaptive droop control for effective power sharing in multi-terminal DC (MTDC) grids," *IEEE Trans. Power Syst.*, vol. 28, no. 1, pp. 21–29, Feb. 2013, doi: 10.1109/TPWRS.2012.2203390.

[52] B. Li, Q. Li, Y. Wang, W. Wen, B. Li, and L. Xu, "A novel method to determine droop coefficients of DC voltage control for VSC-MTDC system," *IEEE Trans. Power Del.*, vol. 35, no. 5, pp. 2196–2211, Oct. 2020, doi: 10.1109/TPWRD.2019.2963447.

[53] R. Eriksson, J. Beerten, M. Ghandhari, and R. Belmans, "Optimizing DC voltage droop settings for AC/DC system interactions," *IEEE Trans. Power Del.*, vol. 29, no. 1, pp. 362–369, Feb. 2014, doi: 10.1109/TPWRD.2013.2264757.

[54] E. Prieto-Araujo, F. D. Bianchi, A. Junyent-Ferre, and O. Gomis-Bellmunt, "Methodology for droop control dynamic analysis of multiterminal VSC-HVDC grids for offshore wind farms," *IEEE Trans. Power Del.*, vol. 26, no. 4, pp. 2476–2485, Oct. 2011, doi: 10.1109/TPWRD.2011.2144625.

[55] E. Prieto-Araujo, A. Egea-Alvarez, S. Fekriasl, and O. Gomis-Bellmunt, "DC voltage droop control design for multiterminal HVDC systems considering AC and DC grid dynamics," *IEEE Trans. Power Del.*, vol. 31, no. 2, pp. 575–585, Apr. 2016, doi: 10.1109/TPWRD.2015.2451531.
[56] O. Yadav, N. Kishor, and R. Negi, "Power imbalance sharing among the power converters in MTDC system," *Int. J. Electr. Power Energy Syst.*, vol. 109, pp. 584–596, Jul. 2019, doi: 10.1016/j.ijepes.2019.02.005.
[57] W. Wang, Y. Li, Y. Cao, U. Hager, and C. Rehtanz, "Adaptive droop control of VSC-MTDC system for frequency support and power sharing," *IEEE Trans. Power Syst.*, vol. 33, no. 2, pp. 1264–1274, Mar. 2018, doi: 10.1109/TPWRS.2017.2719002.
[58] J. Beerten and R. Belmans, "Analysis of power sharing and voltage deviations in droop-controlled DC grids," *IEEE Trans. Power Syst.*, vol. 28, no. 4, pp. 4588–4597, Nov. 2013, doi: 10.1109/TPWRS.2013.2272494.
[59] F. Zhang and Q. Li, "Methodology of calculating droop coefficients for stabilising DC voltage in VSC-MTDC system against disturbances," *IET Gener., Transmiss. Distrib.*, vol. 13, no. 4, pp. 521–535, Feb. 2019, doi: 10.1049/iet-gtd.2018.5058.
[60] S. S. Sayed and A. M. Massoud, "A generalized approach for design of contingency versatile DC voltage droop control in multi-terminal HVDC networks," *Int. J. Electr. Power Energy Syst.*, vol. 126, Mar. 2021, Art. no. 106413, doi: 10.1016/j.ijepes.2020.106413.
[61] L. Xu, L. Yao, and M. Bazargan, "DC grid management of a multi-terminal HVDC transmission system for large offshore wind farms," in *Proc. Int. Conf. Sustain. Power Gener. Supply*, Apr. 2009, pp. 1–7, doi: 10.1109/SUPERGEN.2009.5348101.
[62] P. Simiyu, A. Xin, G. T. Bitew, M. Shahzad, W. Kunyu, and L. K. Tuan, "Review of the DC voltage coordinated control strategies for multi-terminal VSC-MVDC distribution network," *J. Eng.*, vol. 2019, no. 16, pp. 1462–1468, Mar. 2019, doi: 10.1049/joe.2018.8841.
[63] J. Khazaei, Z. Miao, L. Piyasinghe, and L. Fan, "Minimizing DC system loss in multi-terminal HVDC systems through adaptive droop control," *Electr. Power Syst. Res.*, vol. 126, pp. 78–86, Sep. 2015, doi: 10.1016/j.epsr.2015.04.020.
[64] Y. Wang, W. Wen, C. Wang, H. Liu, X. Zhan, and X. Xiao, "Adaptive voltage droop control of multiterminal VSC-HVDC systems for DC voltage deviation and power sharing," *IEEE Trans. Power Deliv.*, vol. 34, no. 1, pp. 169–176, Jun. 2019, doi: 10.1109/TPWRD.2018.2844330.
[65] B. Li, T. Liu, and Y. Zhang, "Unified adaptive droop control design based on dynamic reactive power limiter in VSC-MTDC," *Electr. Power Syst. Res.*, vol. 148, pp. 18–26, Jul. 2017, doi: 10.1016/j.epsr.2017.03.010.
[66] X. Chen, L. Wang, H. Sun, and Y. Chen, "Fuzzy logic based adaptive droop control in multiterminal HVDC for wind power integration," *IEEE Trans. Energy Convers.*, vol. 32, no. 3, pp. 1200–1208, Sep. 2017, doi: 10.1109/TEC.2017.2697967.
[67] R. Wang, L. Chen, T. Zheng, and S. Mei, "VSG-based adaptive droop control for frequency and active power regulation in the MTDC system," *CSEE J. Power Energy Syst.*, vol. 3, no. 3, pp. 260–268, Oct. 2017, doi: 10.17775/CSEEJPES.2017.00040.
[68] S. Sayed and A. Massoud, "Optimal DC voltage control in multi-terminal HVDC network: Modeling and scenarios," in *Proc. IEEE 9th Symp. Comput. Appl. Ind. Electron. (ISCAIE)*, Apr. 2019, pp. 86–91, doi: 10.1109/ISCAIE.2019.8743802.
[69] X. Zhao and K. Li, "Control of VSC-HVDC for wind farm integration based on adaptive backstepping method," in *Proc. IEEE Int. Workshop Inteligent Energy Syst. (IWIES)*, Nov. 2013, pp. 64–69, doi: 10.1109/IWIES.2013.6698563.

SAWSAN S. SAYED received the B.Sc. (Hons.) and M.Sc. degrees in electrical engineering from Qatar University, Qatar, in 2016 and 2018, respectively. She worked as a Graduate Assistant at Qatar University, from 2016 to 2018. She is currently working as a Research Assistant of the National Priorities Research Program, Qatar University. Her research interests include power electronics, renewable energy, energy management, and power systems.

AHMED M. MASSOUD (Senior Member, IEEE) received the B.Sc. (Hons.) and M.Sc. degrees in electrical engineering from Alexandria University, Egypt, in 1997 and 2000, respectively, and the Ph.D. degree in electrical engineering from Heriot-Watt University, Edinburgh, U.K., in 2004. He is currently the Associate Dean for Research and Graduate Studies at the College of Engineering and a Professor at the Department of Electrical Engineering, College of Engineering, Qatar University. His research interests include power electronics, energy conversion, renewable energy, and power quality. He holds eight U.S. patents. He has published more than 100 journal articles in the fields of power electronics, energy conversion, and power quality.